IEEE Access
Multidisciplinary | Rapid Review | Open Access Journal

Received November 18, 2021, accepted January 3, 2022, date of publication January 31, 2022, date of current version March 1, 2022.

Digital Object Identifier 10.1109/ACCESS.2022.3147452

Vehicle Stability Upper-Level-Controller Based on Parameterized Model Predictive Control

ZOÉ ROBERTO MAGALHÃES JÚNIOR[1], ANDRÉ MURILO[2], AND RENATO VILELA LOPES[2]
[1]Departamento de Engenharia Mecanica (ENM)-FT, Universidade de Brasilia (UnB), Campus Darcy Ribeiro, Brasilia 70910-900, Brazil
[2]Faculdade do Gama (FGA), Universidade de Brasilia (UnB), Campus do Gama, Brasilia 72444-240, Brazil

Corresponding author: Zoé Roberto Magalhães Júnior (zr.magal@gmail.com)

This work was supported in part by the Coordination of Superior Level Staff Improvement (CAPES), in part by the National Council for Scientific and Technological Development (CNPq), and in part by the Federal District Research Support Foundation (FAP-DF).

ABSTRACT This paper presents an upper-level vehicular stability controller based on parameterized Model Predictive Control (MPC). The proposed system computes the additional moment applied on the vehicle's yaw axis to improve the lateral stability. In the MPC formulation, the optimization problem is defined as a quadratic programming derived from a linear time-invariant model of vehicle dynamics. The control system is implemented based on a model that considers the rolling movement and on a simpler model that does not consider it, in order to evaluate the effects of using a more representative linear model for more accurate prediction or a simplified model for faster calculation. Constraints are imposed on the optimization problem to deal with the limits in the corrective yaw moment. A parameterized MPC approach is designed to reduce the number of optimization variables, and hence, reducing the computation time required for real-time implementation. Model-in-the-loop simulations are proposed to evaluate the effectiveness of the MPC strategy to avoid steering instability. Simulations are performed for profiling the calculation time, tuning the parameters, and testing algorithm running in an ARM-Cortex A8 on real-time control. Simulation results show that the proposed control strategy is effective in preventing destabilization and demonstrates that even with a longer computation time, the resulting MPC scheme meets the control requirements successfully, even under the presence of model disturbances.

INDEX TERMS Electronic stability control, model predictive control, vehicle lateral stability.

I. INTRODUCTION

Vehicle movement may divert from the driver's intention in adverse driving conditions. Electronic stability control (ESC) systems are active safety systems designed to correct undesired actions that may take the vehicle off the desired path or make driving too complicated for not skillful drivers. They have played a significant role in reducing the risk of fatal car crashes in recent years [1]. Thus, several research topics have been developed to design a proper control structure for these systems. In many cases [2]–[7], a hierarchical architecture is often used, where an upper-level controller calculates a virtual control input (e.g., the direct yaw moment, the tire-slip ratio, the force generated on tires), while a low-level controller commands the available actuation system to change the torque transferred to the wheels, to cause a difference between the forces acting on the tires that ensure the virtual command calculated by the upper-level controller.

The associate editor coordinating the review of this manuscript and approving it for publication was Huiqing Wen.

Regarding control methodologies used in ESC design, advances in computational power of embedded systems have made possible the exploration of different control theories, such as sliding mode control [8]–[11], backstepping technique [12] and robust gain schedule [13], [14].

Another optimal control strategy applicable to ESC's control problem is the Model Predictive Control (MPC). According to MPC definition [15], [16], the controller solves, at each sampling instant, a constrained optimization problem to find the sequence of yaw moments applied to the car at the next sampling instants over a finite prediction horizon. In this process, just the first element of this sequence is applied to the vehicle. In this sense, it may be interesting to consider the potential use of MPC strategies in ESC design, due to its ability to predict future response using vehicle dynamics models and to address the physical limits of actuation. Thus, the MPC has excellent features to meet vehicle stability control requirements.

Indeed, in the literature, some recent contributions emerged concerning MPC for vehicle stability control [17]–[21]. Despite the reasonably satisfactory performances

TABLE 1. Nomenclature.

a	Length from front axis to center of mass	u	Vehicle longitudinal speed
b	Length from rear axis to center of mass	v	Vehicle lateral speed
l	Vehicle total length from rear axis to front axis	ψ	Yaw angle
t_f	Front track width	ϕ	Roll angle
t_r	Rear track width	δ_f	Steering angle of front wheels
h_s	Height of center of mass above rolling center	δ_r	Steering angle of rear wheels
h	Height of center of mass	δ_D	Steering wheel angle
m_s	Sprung mass	F_{yi}	Lateral force generated by tire i
I_{zz}	Yawing inertial moment	γ	Camber angle
I_{xx}	Rolling inertial moment	α_i	Tire slip angle of wheel i
I_{xz}	Inertial product related to yawing and rolling	β	Vehicle side-slip angle
$c_{\phi f}$	Front rolling damping coefficient	g	Gravity acceleration
$c_{\phi r}$	Rear rolling damping coefficient	$C_{\alpha i}$	Cornering stiffness of wheel i
$k_{\phi f}$	Front rolling stiffness coefficient	$C_{\gamma i}$	Camber stiffness
$k_{\phi r}$	Rear rolling stiffness coefficient	K_γ	Camber gradient
$\partial\delta_f/\partial\phi$	Front steer-by-roll coefficient	$\partial\delta_r/\partial\phi$	Rear steer-by-roll coefficient
M_u	Extra yaw moment given as control signal	μ	Tire-road friction coefficient
I_s	Steering coefficient	u_{ref}	Constant longitudinal speed of control set point
$\mathbf{A} \in \mathbb{R}^{4\times4}$	State matrix of state space model	$\mathbf{B} \in \mathbb{R}^{4\times2}$	Input matrix of state space model
$\mathbf{A}_d \in \mathbb{R}^{4\times4}$	State matrix of discrete-time state space model	$\mathbf{B}_d \in \mathbb{R}^{4\times2}$	Input matrix of discrete-time state space model
$\mathbf{x} \in \mathbb{R}^{4\times1}$	State vector of state space model	$\mathbf{u}_c \in \mathbb{R}^{2\times1}$	Input vector of state space model
$\mathbf{\Lambda} \in \mathbb{R}^{4\times1}$	Vector of side-slip of the tires	$\mathbf{F}_y \in \mathbb{R}^{4\times1}$	Vector of lateral forces acting on the tires

of the algorithms used in these works, an issue that must be considered for MPC-based stability control is not taken into account in any of these papers, which is the computational efficiency in real-time applications. In fact, the main drawback of the MPC controller is that running an on-line optimization problem at each time step requires substantial time and computational resources, which is the biggest obstacle to apply this controller to commercial vehicles.

An aspect that affects the MPC's real-time performance is the choice of the prediction model since the use of more simplified models provides less accurate predictions. In contrast, the use of more precise and complex models reduces the commands update rate by increasing the processing time to solve the optimization problem. In general, more accurate predictions are obtained using a nonlinear model to represent vehicle dynamics. However, those models result in nonlinear programming that is a computationally hard problem and is often impractical in real-time applications [17].

In this sense, the main strategy used in the literature is to use a linear model for prediction helps to fit the optimization into the quadratic programming (QP) form. However, the complexity of the QP problem is still a challenge for real-time MPC applications with low-cost hardware. For example, in [18], [22], reconfigurable MPC-based ESCs are proposed to vehicles with different actuation systems. The MPC is designed based on a linear model that considers the roll motion and can predict the response to different combinations of control inputs. The set-up is performed by setting a selector matrix that makes the prediction model unresponsive to unavailable control inputs, without taking off those inputs from the linear model, which does not affect the length of the Hessian matrix of the optimization problem. Simulations are performed to demonstrate the effectiveness of proposed ESCs with different configurations. However, the implementation of the embedded control system to execute the proposed algorithm is not presented, as well as no simplification of the optimization problem is applied to the QP to improve the computation time required to solve it.

Stability control based on MPC to handle with constraints on control inputs has been presented in [20], [23]–[25]. In [20], [23], [24], the rotations of the wheels are included as state variables of the prediction model, and in [25], the slip angles of the rear and front axis are considered. Results from simulation and experimental tests are presented to demonstrate the effectiveness of proposed ESCs to improve vehicle stability. However, real-time implementation issues are not addressed.

An unconstrained MPC for yaw stability with practical concerns is presented in [26], where the cost function of MPC is defined without inequality constraints such that a closed-form solution can be defined as the optimization problem. Therefore, the computational efficiency of ESC is improved by avoiding the QP solving. Nevertheless, the proposed approach excludes the MPC capability to handle the constraints of the actuation system.

In [5], an MPC is designed to integrate the objectives of the longitudinal collision avoidance and lateral stability. The algorithm dynamically alters the weight matrices of the QP problem according to driving conditions. The MPC is designed based on the two-degree-of-freedom (DOF) vehicle's lateral model that includes only the yaw rate and the side-slip of the vehicle body. Hardware-in-the-loop (HIL) simulations are performed in a platform where the vehicle motion and the control algorithm are simulated by computers that access from a Controller Area Network (CAN) bus a brake system, a yaw rate sensor, and a wheel-speed simulator. Again, the embedded control system is also not presented, and no method is shown to reduce MPC's computation time.

Thus, it is worth mentioning the lack in the literature regarding contributions that address the real-time implementation of a constrained MPC-based ESC with lim-

ited processing hardware. In this context, the present paper proposes a constrained parameterized MPC-based upper-level ESC that computes the additional yaw moment to improve lateral stability. Therefore, this can be used as input for a low-level controller that commands an available actuation system able to generate a moment at the vehicle yaw axis. To reduce the complexity of the optimization problem, the MPC is designed using the parameterization of the input vector to reduce the number of optimization variables and, hence, the computation time.

The reduction in processing time allows us to investigate the advantages of using a more representative prediction model for lateral stability control. Thus two versions of the control system proposed in this paper are implemented using different prediction models: a more realist one that uses the rolling motion and a simpler one that does not consider it. Although the objective of this work is not to propose a system that integrates the stability control and rollover prevention, the implementation of the MPC using a linear model that includes the rolling movements, in addition to providing a more realistic prediction, enables some roll control. This capability can be used to avoid solutions that improve lateral stability performance at the cost of a significant increase in rollover risk.

Lateral stability controllers based on linear models that include the roll motion have been presented in [4], [18], [22], [27], [28]. In [4], [18], [22], [27], The MPC is implemented with an optimization problem defined to combine the objectives of the rollover prevention and lateral stability control. And [28] introduces an index to measure the loss of adhesion between the tire and the road, which, along with a rollover index, is used to define the objectives of a robust control developed to mitigate the accident risk. Nevertheless, such papers do not present the effects on the stability performance in comparison with the use of a simpler model taking into account the computation time.

Therefore, the main contribution of this paper consists of designing a computational efficient MPC strategy that reduces the complexity of solving the optimization problem by applying an exponential parameterization to the control vector over the prediction horizon. In addition to that, this paper also presents:

- The implementation and testing of a parameterized MPC strategy embedded on BeagleBoneBlack Rev C.
- Tuning and evaluation of MPC with Processor-in-the-loop (PIL) simulations, enabling validation, and implementation of the embedded controller in real hardware with limited resources and processing capacity.
- Comparison results for lateral stability between the proposed MPC strategy and Linear Quadratic Regulator (LQR), which is more computationally efficient but unable to handle with system's constraints.
- Comparison results for lateral stability between two versions of the proposed ESC based on different prediction models: one simplified model that includes only the side-slip angle and the yaw rate, and another that adds the roll angle and the roll rate within the states.

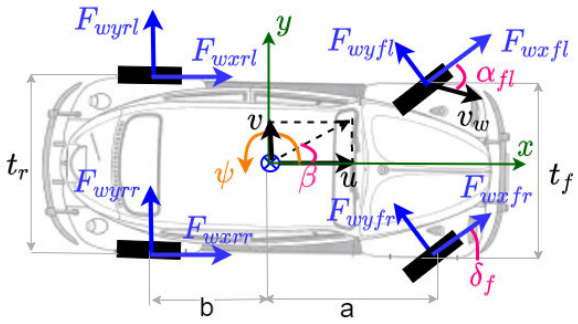

FIGURE 1. Schematic view of vehicle dynamic model.

This paper is organized as follows. First, the vehicle model is presented in section II. Then the control problem is presented in section III. The parameterized MPC scheme is then detailed in section IV. Section V presents the methodology used for experiments with a complete hardware description. Simulation and experimental results are presented in section VI. This paper ends with conclusions and future works in section VII.

II. VEHICLE DYNAMICS

The vehicle dynamics model considered in this work for implementation of simulations environments and for obtaining the linear model used in control design includes the lateral, yaw and roll motions, and assumes a constant longitudinal speed [4], [29]–[31]. Figure 1 shows this model represented by the following equations of motions:

$$\begin{aligned} m\left(\dot{v}-\dot{\psi}u\right)-m_s h_s\ddot{\phi} &= \sum F_y \\ I_{zz}\ddot{\psi}-I_{xz}\ddot{\phi} &= \sum M_z \\ I_{xx}\ddot{\phi}-I_{xz}\ddot{\psi} &= \sum M_x \end{aligned} \tag{1}$$

where v denotes the lateral speed, u the longitudinal speed, ϕ the roll angle, ψ the yaw angle, m the vehicle total mass, m_s the sprung mass, h_s the sprung height, I_{xx} and I_{zz} the yawing and rolling inertial moments, respectively, I_{xz} the inertial product related to yawing and rolling. F_y, the lateral forces generated by tires on vehicle's center of gravity (CG), M_z are M_x are the moments on yaw and roll axes, respectively.

The lateral forces and moments on vehicle CG are resultant of the forces acting on tires, are obtained as follows:

$$\begin{aligned} \sum F_y &= F_{yfl}+F_{yfr}+F_{yrl}+F_{yrr} \\ \sum M_z &= a\left(F_{yfl}+F_{yfr}\right)-b\left(F_{yrl}+F_{yrr}\right) \\ &\quad +\frac{t_f}{2}\left(F_{xfr}-F_{xfl}\right)-\frac{t_r}{2}\left(F_{xrr}-F_{xrl}\right)+M_u \\ \sum M_x &= m_s h_s\left(\dot{v}+\dot{\psi}u\right)+m_s h_s g\sin(\phi) \\ &\quad -\left(k_{\phi f}+k_{\phi r}\right)\phi-\left(c_{\phi f}+c_{\phi r}\right)\dot{\phi} \end{aligned} \tag{2}$$

where a denotes the distance from front axis to CG, b the distance from rear axis to CG, t_f and t_r the front and rear track width, respectively, M_u the extra yaw-moment, $k_{\phi f}$ and $k_{\phi r}$ the front and rear roll stiffness coefficient, respectively, $c_{\phi f}$ and $c_{\phi r}$ the front and rear roll dumping coefficient, respectively. F_{yfl}, F_{yfr}, F_{yrl}, and F_{yrr} are the components of the forces generated by front-left, front-right, rear-left, and rear-right tires in the direction of lateral axis of the vehicle. And F_{xfl}, F_{xfr}, F_{xrl}, and F_{xrr} are the component of forces generated by front-left, front-right, rear-left, and rear-right tires in the direction of longitudinal axis of the vehicle.

The projection of the forces acting on tires on the longitudinal and lateral axes of the vehicle depends on the steering angle of the wheels, and it is given by the following equation of vector rotation:

$$\begin{bmatrix} F_{xi} \\ F_{yi} \end{bmatrix} = \begin{bmatrix} cos(\delta_i) & sin(\delta_i) \\ -sin(\delta_i) & cos(\delta_i) \end{bmatrix} \cdot \begin{bmatrix} F_{wxi} \\ F_{wyi} \end{bmatrix} \tag{3}$$

where $i \in fl, fr, rl, rr$, in which fl, fr, rl, rr index the front-left, front-right, rear-left and rear-right tires, respectively, and δ_i is the steering angle of i^{th} tire.

A constant longitudinal speed means no longitudinal acceleration, which means that there is a balance between the forces on longitudinal direction generated by tires and friction. For approximation, it is considering that such balance is obtained because the longitudinal forces acting on each tire are the same. In this way, the longitudinal forces of the tires cancel out each other in the in the yaw moment equation in (2). And that is the reason why the longitudinal forces of the tires are not included in this model [25], [32]–[34].

A metric to analyze lateral stability performance is the side-slip angle β, which is the angle between the total speed and vehicle's longitudinal axis, such as $\beta = \arctan v/u$. It is a measure of how much the vehicle is laterally slipping from the desired trajectory.

A. TIRE DYNAMICS

The Pacejka's Magic Formula (MF) is an empirical formulation derived from experimental tests that can be used to compute forces acting on tires [35]. Using Pacejka's MF, the lateral force F_{yi} and the longitudinal force F_{xi} acting in each tire, indexed by i, can be obtained from values of wheel vertical force F_{zi}, tire slip angle α_i, camber angle γ_i, and slip ration λ as follows:

$$\begin{aligned}
F_{yi} &= D\sin(Sv_i + C\arctan[B(1-E)\alpha_i' + E\arctan(B\alpha_i')]) \\
C &= a_0 \\
D &= F_{zi}(a_1 F_{zi} + a_2) \\
B &= \frac{a_3 \sin(2\arctan\frac{F_{zi}}{a_4})}{CD}(1 - a_5|\gamma_i|) \\
E &= a_6 F_{zi} + a_7 \\
Sh_i &= a_8\gamma_i + a_9 F_{zi} + a_{10} \\
Sv_i &= \left(a_{11}F_{zi}^2 + a_{12}F_{zi}\right)\gamma_i + a_{13}F_{zi} + a_{14} \\
\alpha_i' &= \alpha_i + Sh_i
\end{aligned}$$

$$i = fl, fr, rl, rr \tag{4}$$

$$\begin{aligned}
F_{xi} &= D\sin(Sv_i + C\arctan[B(1-E)\lambda_i' + E\arctan(B\lambda_i')]) \\
C &= b_0 \\
D &= F_{zi}(b_1 F_{zi} + b_2) \\
B &= \frac{b_3 \sin(2\arctan\frac{F_{zi}}{b_4})\exp(b_5 F_{zi})}{CD} \\
E &= b_6 F_{zi}^2 + b_7 F_{zi} + b_8 \\
Sh_i &= b_9 F_{zi} + b_{10} \\
Sv_i &= 0
\end{aligned}$$

$$i = fl, fr, rl, rr \tag{5}$$

where $a_1, a_2, a_3, \ldots, a_{14}$ and $b_1, b_2, b_3, \ldots, b_{10}$ are the Pacejka's Magic Formula coefficients [35].

The side-slip angle is the angle between the tire's longitudinal axis and its velocity vector. The side-slip angle of the front-left tire α_{lf} is illustrated in Figure 1. The side-slip angle of the four tires are given by:

$$\begin{aligned}
\alpha_{fl} &= \delta_f - \arctan\left(\frac{v + a\dot{\psi}}{u - \frac{t_f}{2}\dot{\psi}}\right) \\
\alpha_{fr} &= \delta_f - \arctan\left(\frac{v + a\dot{\psi}}{u + \frac{t_f}{2}\dot{\psi}}\right) \\
\alpha_{rl} &= -\arctan\left(\frac{v - b\dot{\psi}}{u - \frac{t_r}{2}\dot{\psi}}\right) \\
\alpha_{rr} &= -\arctan\left(\frac{v - b\dot{\psi}}{u + \frac{t_r}{2}\dot{\psi}}\right)
\end{aligned} \tag{6}$$

The slip ratio is the relative difference of the rolling speed of the tire and the vehicle's longitudinal speed, and its given by:

$$\lambda_i = \begin{cases} \dfrac{\omega R_{eff} - u}{\omega_i R_{eff}}, & \text{if } \omega_i R_{eff} > u \\ \dfrac{u - \omega_i R_{eff}}{u}, & \text{otherwise} \end{cases} \tag{7}$$

in which ω_i is the angular speed of the wheel, R_{eff} is the effective radius of the wheel-tire set, and u is the vehicle longitudinal speed.

The vertical load on each wheel is given by the vehicle weight transferred to it. When vehicle is moving, the vertical force in each wheel are given by [4], [31]:

$$\begin{aligned}
F_{zfl} &= \frac{mgb}{2l} - \frac{ma_x h}{2l} - \frac{ma_y ah}{lt_f} - \frac{k_{\phi f}\phi}{t_f} - \frac{c_{\phi f}\dot{\phi}}{t_f} \\
F_{zfr} &= \frac{mgb}{2l} - \frac{ma_x h}{2l} + \frac{ma_y ah}{lt_f} + \frac{k_{\phi f}\phi}{t_f} + \frac{c_{\phi f}\dot{\phi}}{t_f} \\
F_{zrl} &= \frac{mga}{2l} + \frac{ma_x h}{2l} - \frac{ma_y ah}{lt_r} - \frac{k_{\phi r}\phi}{t_r} - \frac{c_{\phi r}\dot{\phi}}{t_r} \\
F_{zrr} &= \frac{mga}{2l} + \frac{ma_x h}{2l} + \frac{ma_y ah}{lt_r} + \frac{k_{\phi r}\phi}{t_r} + \frac{c_{\phi r}\dot{\phi}}{t_r}
\end{aligned} \tag{8}$$

in the above equations, h denotes the height of the center of gravity, and l the wheelbase.

In this work, to take into account the effects of roll motion on tire dynamic, the camber angle of four wheels are considered ideally the same, simplified as follows:

$$\gamma = K_\gamma \phi \tag{9}$$

K_γ denotes the camber-by-roll gradient, which represents variation of camber due to rolling given by $K_\gamma = \frac{\partial \gamma}{\partial \phi}$ [36]. The steering angle of wheels is obtained by summing a part relating to the driver's command and a component generated by rolling motion. For a passenger car, where the steering wheel controls only the front wheels, the front, and rear steer angles can be obtained as follows:

$$\begin{bmatrix} \delta_{fl} \\ \delta_{fr} \\ \delta_{rl} \\ \delta_{rr} \end{bmatrix} = \mathbf{G}_\delta \delta_D + \begin{bmatrix} \frac{\partial \delta_f}{\partial \phi} \\ \frac{\partial \delta_f}{\partial \phi} \\ \frac{\partial \delta_r}{\partial \phi} \\ \frac{\partial \delta_r}{\partial \phi} \end{bmatrix} \phi$$
$$\mathbf{G}_\delta = \begin{bmatrix} 1/I_s & 1/I_s & 0 & 0 \end{bmatrix}^T \tag{10}$$

where δ_D is the steering wheel angle, I_s is the steering coefficient, and $\partial \delta_r / \partial \phi$ and $\partial \delta_f / \partial \phi$ are rear and front steer-by-roll coefficient, respectively.

B. LINEAR MODEL

In the literature on lateral stability control, the vehicle linear model used in control design is often obtained from simplifications for constant longitudinal speed $u = u_{ref}$ and small angles [18], [22], [37], such that $\sin(\phi) \approx \phi$, $\sin(\delta_i) \approx \delta_i$, $\cos(\delta_i) \approx 1$, and $\beta \approx v/u_{ref}$. This strategy is used in this work to obtain the linear model used in MPC implementation from linearization of the presented non-linear model. Thus, the linearization of the equations of motion (Eq. 1 and Eq. 2) is given by:

$$\mathbf{K}_\mathbf{x} \dot{\mathbf{x}} = \mathbf{G}_\mathbf{x} \mathbf{x} + \mathbf{G}_F \mathbf{F}_y + \mathbf{G}_u M_u$$
$$\mathbf{x} = \begin{bmatrix} \beta & \dot{\psi} & \dot{\phi} & \phi \end{bmatrix}^T$$
$$\mathbf{F}_y = \begin{bmatrix} F_{yfl} & F_{yfr} & F_{yrl} & F_{yrr} \end{bmatrix}^T$$
$$\mathbf{K}_\mathbf{x} = \begin{bmatrix} mu_{ref} & 0 & -m_s h_s & 0 \\ 0 & I_{zz} & -Ixz & (c_{\phi f} + c_{\phi r}) \\ -m_s h_s u_{ref} & I_{xz} & I_{xx} & 0 \\ 0 & 0 & 0 & 1 \end{bmatrix}$$
$$\mathbf{G}_x = \begin{bmatrix} 0 & -mu_{ref} & 0 & 0 \\ 0 & 0 & 0 & 0 \\ 0 & m_s h_s u_{ref} & 0 & (m_s h_s g - k_{\phi f} - k_{\phi r}) \\ 0 & 0 & 1 & 0 \end{bmatrix}$$
$$\mathbf{G}_F = \begin{bmatrix} 1 & 1 & 1 & 1 \\ a & a & -b & -b \\ 0 & 0 & 0 & 0 \\ 0 & 0 & 0 & 0 \end{bmatrix}$$
$$\mathbf{G}_u = \begin{bmatrix} 0 & 1 & 0 & 0 \end{bmatrix}^T \tag{11}$$

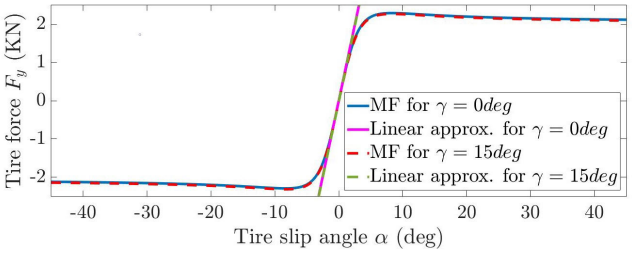

FIGURE 2. Lateral tire forces computed by Magic formula of Pacejka and its linear approximation.

The consideration of small angles places the linearization point within the stability zone so that while the control is successful in preventing instability, the vehicle's response remains close to that predicted by the linear model. A drawback of this approach consists in considering the constant speed in the linear model so that whenever the vehicle speed is different from the linearization point, there will be a mismatch between the vehicle's response and that predicted by the model.

Equation 11 presents a linear model of the movement response to the lateral forces generated in each tire. Thus, the second stage of linearization consists of obtaining a linear model of the forces generated in the tires. For small tire slip and camber angles, a good approximation of the force generated in the tires is given by [30], [35]:

$$F_{yi} = C_{\alpha i} \alpha_i + C_{\gamma i} \gamma$$
$$C_{\alpha i} = \left. \frac{\partial F_{yi}}{\partial \alpha_i} \right|_{a_x, a_y, \gamma, \alpha, \phi, \dot{\phi} = 0}$$
$$C_{\gamma i} = \left. \frac{\partial F_{yi}}{\partial \gamma_i} \right|_{a_x, a_y, \gamma, \alpha, \phi, \dot{\phi} = 0}$$
$$i = fl, fr, rl, rr \tag{12}$$

where $C_{\alpha i}$ and $C_{\gamma i}$ denote cornering stiffness and camber stiffness coefficients, which can be obtained from Equations (4) and (12) [35]. Fig. 2 shows the forces generated by the MF and this linear approximation, where one can see that for small angles the Equation (12) gives a good approximation.

Replacing the Equation (9) in (12), the vector F_Y of lateral forces generated on tires can be expressed as:

$$\mathbf{F}_y = \mathbf{G}_\alpha \mathbf{\Lambda} + \mathbf{G}_\gamma \mathbf{x}$$
$$\mathbf{\Lambda} = \begin{bmatrix} \alpha_{fl} & \alpha_{fr} & \alpha_{rl} & \alpha_{rr} \end{bmatrix}^T$$
$$\mathbf{G}_\alpha = \begin{bmatrix} C_{\alpha fl} & C_{\alpha fr} & C_{\alpha rl} & C_{\alpha rr} \end{bmatrix}$$
$$\mathbf{G}_\gamma = \begin{bmatrix} 0_{1\times 3} & C_{\gamma fl} K_\gamma \\ 0_{1\times 3} & C_{\gamma fr} K_\gamma \\ 0_{1\times 3} & C_{\gamma rl} K_\gamma \\ 0_{1\times 3} & C_{\gamma rr} K_\gamma \end{bmatrix} \tag{13}$$

The front and rear wheels slip angle are approximated by linear functions of vehicle slip angle, yaw rate, and wheels

steer angle [21], [31]:

$$\mathbf{\Lambda} = \begin{bmatrix} -1 & -a/u & 0 & 0 \\ -1 & -a/u & 0 & 0 \\ -1 & b/u & 0 & 0 \end{bmatrix} \mathbf{x} + \begin{bmatrix} \delta_{fl} \\ \delta_{fr} \\ \delta_{rl} \\ \delta_{rr} \end{bmatrix} \tag{14}$$

Combining Equations (10) and (14), the following equation is obtained:

$$\begin{aligned} \mathbf{\Lambda} &= \mathbf{G}_\Lambda \mathbf{x} + \mathbf{G}_\delta \delta_D \\ \mathbf{G}_\Lambda &= \begin{bmatrix} -1 & -a/u & 0 & \frac{\partial \delta_f}{\partial \phi} \\ -1 & -a/u & 0 & \frac{\partial \delta_f}{\partial \phi} \\ -1 & b/u & 0 & \frac{\partial \delta_r}{\partial \phi} \\ -1 & b/u & 0 & \frac{\partial \delta_r}{\partial \phi} \end{bmatrix} \end{aligned} \tag{15}$$

The linear model of vehicle dynamics in the state space form can be obtained by combining equations from (11) to (15):

$$\begin{aligned} \dot{\mathbf{x}} &= \mathbf{A}\mathbf{x} + \mathbf{B}\mathbf{u}_c \\ \mathbf{u}_c &= \begin{bmatrix} M_u & \delta_D \end{bmatrix}^T \\ \mathbf{A} &= \mathbf{K}_x^{-1} \left[\mathbf{G}_x + \mathbf{G}_F \left(\mathbf{G}_\alpha \mathbf{G}_\Lambda + \mathbf{G}_\gamma \right) \right] \\ \mathbf{B} &= \mathbf{K}_x^{-1} \left[\mathbf{G}_u \ \mathbf{G}_F \mathbf{G}_\alpha \mathbf{G}_\gamma \mathbf{G}_\delta \right] \end{aligned} \tag{16}$$

The resulting linear model (16) is fully controllable since the controllability matrix obtained from the pair $(\mathbf{A}, \mathbf{B}^*)$, with $\mathbf{B}^* = \mathbf{K}_x^{-1}\mathbf{G}_u$ related to the controllable input M_u, is of full rank.

III. CONTROL PROBLEM

This high-level controller is designed to compute moment applied on yaw axis to keep the steering stability. This corrective yaw moment is resultant of differences in the tire's longitudinal forces on left and right sides of vehicle. Since there is a limit for the forces generated on tires, there are constraints for the corrective yaw moment that must be taken into account by the control algorithm. This imposes that the control input M_u must satisfy:

$$M_u^{min} \leq M_u \leq M_u^{max} \tag{17}$$

There is also a limit to the difference between consecutive command updates. The design of high-level control does not consider a specific actuation system. However, the control algorithm must be able to take into account this limitation, and thus the control input must satisfy:

$$\Delta M_u^{min} \leq (M_u(k) - M_u(k-1)) \leq \Delta M_u^{max} \tag{18}$$

The corrective yaw moment is defined as the one that minimizes a cost function that includes the actuation energy and the yaw error error over a finite horizon, which are predicted based on the linear model presented in Section II-B. This cost function and the optimization problem is formulated as a quadratic programming by following the MPC method.

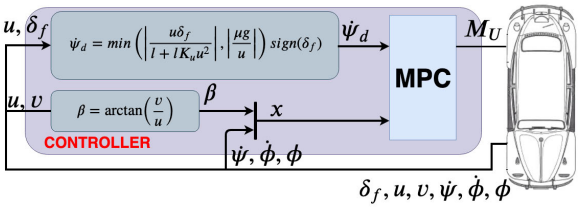

FIGURE 3. Block diagram of control system.

IV. CONTROL DESIGN

The architecture of the proposed control system is presented in Fig. 3. The MPC receives the current and desired states, and calculates the corrective yaw moment required to keep the steering stable. It is assumed that measures of yaw rate, roll rate, and roll angle are available, whereas side-slip angle is calculated from measures of lateral and front speed.

In the formulation of the MPC, the controller must define, at each instant of sampling, the desired value of the regulated states over the prediction horizon. In the optimal configuration, obtained from the tuning of MPC coefficients presented in Section VI-A, only the yaw and roll rates are included within the regulated states. As rolling is an unwanted movement that increases the rollover risk and decreases passenger comfort, the desired roll rate is assumed equal to zero over the prediction horizon, such that the cost function of the optimization problem penalizes any value different from zero. The desired yaw rate depends on the steering wheel angle commanded by the driver in response to vehicle movement. For a given vehicle, characterized by its geometric parameters and cornering stiffness coefficients, the desired yaw rate can be computed as follows [31]:

$$\begin{aligned} \dot{\psi}_d &= min\left(\left| \frac{u\delta_f}{l + lK_u u^2} \right|, \left| \frac{\mu g}{u} \right| \right) sign(\delta_f) \\ K_u &= \frac{m}{l^2} \left(\frac{b}{C_{\alpha r}} - \frac{a}{C_{\alpha f}} \right) \end{aligned} \tag{19}$$

A. MPC FORMULATION

The MPC method used in this paper follows the formulation presented by [16]. This method needs a discrete linear model of vehicle dynamics, which is obtained from the discretization of the linear model presented in Section II, and represented by:

$$\mathbf{x}(k+1) = \mathbf{A}_d \mathbf{x}(k) + \mathbf{B}_d \mathbf{u}_c(k) \tag{20}$$

where $x(k)$ and $u(k)$ are the state and input at sampling instant k, respectively, and $\mathbf{A}_d \in \mathbb{R}^{4\times4}$ and $\mathbf{B}_d \in \mathbb{R}^{4\times2}$ are state and input discrete matrices, respectively. The next control sequence over a prediction horizon N and the next states, obtained by applying this control sequence, are represented

by:

$$\tilde{\mathbf{u}}(k) = \begin{bmatrix} \mathbf{u}(k) \\ \mathbf{u}(k+1) \\ \vdots \\ \mathbf{u}(k+N-1) \end{bmatrix} \tag{21}$$

$$\tilde{\mathbf{x}}(k) = \begin{bmatrix} \mathbf{x}(k+1) \\ \mathbf{x}(k+2) \\ \vdots \\ \mathbf{x}(k+N) \end{bmatrix} \tag{22}$$

As shown in [16] the states at any sampling instant over the prediction horizon can be obtained from the current states and the future control sequence:

$$\mathbf{x}(k+1) = \mathbf{\Phi}_i \mathbf{x}(k) + \mathbf{\Psi}_i \tilde{\mathbf{u}}(k) \tag{23}$$

where $\mathbf{\Phi}_i \in \mathbb{R}^{4\times 2}$ and $\mathbf{\Psi}_i \in \mathbb{R}^{4\times n_{\tilde{u}}}$ are the state and input prediction matrices, respectively, which can be computed from discrete model matrix as follows:

$$\mathbf{\Phi}_i = \mathbf{A}_d^i \tag{24}$$

$$\mathbf{\Psi}_i = \begin{pmatrix} \mathbf{A}_d^{i-1}\mathbf{B}_d & \dots & \mathbf{A}_d\mathbf{B}_d & \mathbf{B}_d \end{pmatrix}^T \begin{pmatrix} \mathbf{\Pi}_1^{(2,N)} \\ \mathbf{\Pi}_2^{(2,N)} \\ \vdots \\ \mathbf{\Pi}_i^{(2,N)} \end{pmatrix} \tag{25}$$

$$\mathbf{\Pi}_i^{(n,N)} = \begin{pmatrix} 0_{n\times n(i-1)} & I_{n\times n} & 0_{n\times n(N-i)} \end{pmatrix} \tag{26}$$

The regulated output vector can be any linear combination of the states. The proposed ESC directly controls the yaw rate and roll angle, therefore the regulated output is defined as follows:

$$\begin{aligned} \mathbf{y}(k) &= \begin{pmatrix} \dot{\psi} & \phi \end{pmatrix}^T = \mathbf{C}_r \mathbf{x}(k) \\ \mathbf{C}_r &= \begin{bmatrix} 0 & 1 & 0 & 0 \\ 0 & 0 & 0 & 1 \end{bmatrix} \end{aligned} \tag{27}$$

The cost function of MPC formulation is defined depending on current states $x(k)$, desired output $y_d(k) = (\phi_d \quad 0)$ and desired input u_d. This can be expressed as:

$$J(k) = \sum_{i+1}^{N} \left|\mathbf{y}_r(k+i) - \mathbf{y}_d(k+i)\right|_{\mathbf{Q}_y}^2 + \sum_{i+1}^{N} \left|\mathbf{\Pi}_i^{(2,N)}\tilde{\mathbf{u}}(k) - \mathbf{u}_d\right|_{\mathbf{Q}_u}^2 \tag{28}$$

in which, $\mathbf{Q}_u$ and $\mathbf{Q}_y$ are the matrices that weight the energy of command and the errors of regulated output, respectively, and $\mathbf{u_d}$ the desired input. The desired yaw moment is assumed to be zero and for the uncontrolled input, δ_D the desired value is its current value.

The Equation (28) can be expanded in the classical representation of quadratic programming with $\tilde{\boldsymbol{u}}$ as a decision variable:

$$J(k) = \frac{1}{2}\tilde{\mathbf{u}}^T(k)\mathbf{H}\tilde{\mathbf{u}}(k) + \mathbf{F}^T(k)\tilde{\mathbf{u}}(k) \tag{29}$$

where

$$\begin{aligned} \mathbf{H} &= 2\sum_{i=1}^{N}\left[\mathbf{\Phi}_i^T\mathbf{C}_r^T\mathbf{Q}_y\mathbf{C}_r\mathbf{\Psi}_i + (\mathbf{\Psi}_i^{(2,N)})^T\mathbf{Q}_u(\mathbf{\Psi}_i^{(2,N)})\right] \\ \mathbf{F}(k) &= \mathbf{F}_1\mathbf{x}(k) + \mathbf{F}_2\mathbf{y}_d + \mathbf{F}_3\mathbf{y}_d \\ \mathbf{F}_1 &= 2\sum_{i=1}^{N}\mathbf{\Phi}_i^T\mathbf{C}_r^T\mathbf{Q}_y\mathbf{C}_r\mathbf{\Phi}_i \\ \mathbf{F}_2 &= -2\sum_{i=1}^{N}\mathbf{\Phi}_i^T\mathbf{C}_r^T\mathbf{Q}_y\mathbf{C}_r\mathbf{\Pi}_i^{(2,N)} \\ \mathbf{F}_3 &= 2\sum_{i=1}^{N}(\mathbf{\Pi}_i^{(2,N)})^T\mathbf{Q}_u \end{aligned} \tag{30}$$

The next step consists in defining the constraints on the controlled and uncontrolled input variables. The MPC formulation developed in this paper includes δ_D as part of the command vector, however the ESC has no direct control of the steering angle. To handle this scenario, the optimal δ_D computed by the MPC is constrained such that the only possible optimal solution is equal to its current measured value. Thus, one can define the constraints on the input variables and its rates of change as follows:

$$\begin{aligned} \begin{bmatrix} M_u^{min} \\ \delta_D(k-1) \end{bmatrix} &\leq \mathbf{u}_c(k) \leq \begin{bmatrix} M_u^{max} \\ \delta_D(k-1) \end{bmatrix} \\ \begin{bmatrix} \Delta M_u^{min} \\ 0 \end{bmatrix} &\leq \mathbf{u}_c(k+1) - \mathbf{u}_c(k) \leq \begin{bmatrix} \Delta M_u^{max} \\ 0 \end{bmatrix} \end{aligned} \tag{31}$$

The above expression also imposes that the MPC assumes that the uncontrolled input δ_D is constant over the prediction horizon.

B. MPC PARAMETERIZATION

In [16], parameterizations of MPC are proposed to increase the computational efficiency by reducing the number of variables of QP solution. In the proposed controller employs the exponential parameterization, in which the solution of the optimal control inputs over the predication horizon are restrict to the sum of few exponential terms:

$$\begin{bmatrix} M_u(k+i) \\ \delta_D(k+i) \end{bmatrix} = \begin{bmatrix} p_1(k)e^{-\nu T_s i} + p_2(k)e^{-\nu T_s i/(1+\alpha)} \\ p_\delta(k) \end{bmatrix} \tag{32}$$

where k is the discrete time index that starts the prediction horizon, ν and α are constant coefficients of exponential parameterization, T_s is the sampling time, and p_1, p_2 and p_δ are the parameters to be optimized by the MPC algorithm. Thus, instead of optimizing the whole control sequence $\tilde{\mathbf{u}}(k)$ over the prediction horizon, the MPC needs to optimize just the parameter vector defined by $\mathbf{p}(k) = \begin{bmatrix} p_1(k) & p_2(k) & p_\delta(k) \end{bmatrix}^T$. Following this definition, the parameterized control vector is defined by:

$$\begin{aligned} \mathbf{u}_c(k+i) &= \begin{bmatrix} M_u(k+i) \\ \delta_D(k+i) \end{bmatrix} = \mathbf{M}(i)\mathbf{p}(k) \\ \mathbf{M}(i) &= \begin{bmatrix} e^{-\nu T_s i} & e^{-\nu T_s i/(1+\alpha)} & 0 \\ 0 & 0 & 1 \end{bmatrix} \end{aligned} \tag{33}$$

And the parameterized control sequence over the prediction horizon defined in Equation (21) can be expressed as fallows:

$$\tilde{\mathbf{u}}(k) = \mathbf{\Pi}_e \mathbf{p}(k) \qquad \mathbf{\Pi}_e = \begin{bmatrix} M(0) \\ \vdots \\ M(N-1) \end{bmatrix} \tag{34}$$

As the target result of this parameterization, the cost function presented in Equation (28) comes down to a QP in terms of $\mathbf{p}$(k), i.e.:

$$\begin{aligned} J(k) &= \frac{1}{2}\mathbf{p}^T(k)\mathbf{H}_p\mathbf{p}(k) + F_p^T(k)\mathbf{p}(k) \\ \mathbf{H}_p &= \mathbf{\Pi}_e^T H \mathbf{\Pi}_e \\ \mathbf{F}_p(k) &= \mathbf{F}_{p1}\mathbf{x}(k) + \mathbf{F}_{p2}\mathbf{y}_d + \mathbf{F}_{p3}\mathbf{u}_d \\ \mathbf{F}_{p1} &= \mathbf{\Pi}_e^T \mathbf{F}_1 \\ \mathbf{F}_{p2} &= \mathbf{\Pi}_e^T \mathbf{F}_2 \\ \mathbf{F}_{p3} &= \mathbf{\Pi}_e^T \mathbf{F}_3 \end{aligned} \tag{35}$$

And the constraints to control inputs presented in Equation (31) lead to the following constraints for the parameter vector:

$$\begin{aligned} \mathbf{\Pi}_e \begin{bmatrix} M_u^{min} \\ \delta_D(k-1) \end{bmatrix} &\leq \mathbf{\Pi}_e \mathbf{p}(k) \leq \mathbf{\Pi}_e \begin{bmatrix} M_u^{max} \\ \delta_D(k-1) \end{bmatrix} \\ \mathbf{\Pi}_e \begin{bmatrix} \Delta M_u^{min} \\ 0 \end{bmatrix} &\leq \mathbf{\Pi}_e(\mathbf{p}(k+1) - \mathbf{p}(k)) \leq \mathbf{\Pi}_e \begin{bmatrix} \Delta M_u^{max} \\ 0 \end{bmatrix} \end{aligned} \tag{36}$$

And since the solution of the steering input is restrict to its value measured at the beginning of the prediction horizon, the solution is also constrained to $p_\delta = \delta_D(k)$.

The stability of parameterized control schemes was presented in [38], and the necessary and sufficient conditions regarding the classical structure of the MPC were formalized in the survey paper [15]. Such a situation requires a substantial constraint at the final state with longer horizons of prediction (tending to infinity) together with a penalty at the end of the predicted trajectory. Besides, another necessary condition generally requires weighting over the whole state vector along the prediction trajectory. Thus, according to [16], practical and feasible conditions for obtaining all necessary and sufficient conditions for MPC-type strategies can be quite challenging to obtain. As far as embedded systems are concerned, such a scenario can prevent practical implementation of the MPC scheme since the resulting controller may become unfeasible for real-time applications. For this reason, an analysis of the influence of the prediction horizon N as a function of the minimum computation time required to carry out the optimization process efficiently is shown later.

C. ESC ACTIVATION CRITERIA

The MPC may give a non-zero command when the error of regulated states is non-zero. To avoid unnecessary actuation in maneuvers which states are different from its desired values, without risk of the driver losing control of the steering, the ESC control is kept inactive when side-slip angle and yaw error is not greater than a threshold. To avoid constant switching of control activation, the ESC is activated when the condition $\beta > \beta_{th}$ or $\psi_e > \psi_{eth}$ is fulfilled for a minimum period T_{on}, and it is deactivated when it is not fulfilled for a minimum period T_{off}.

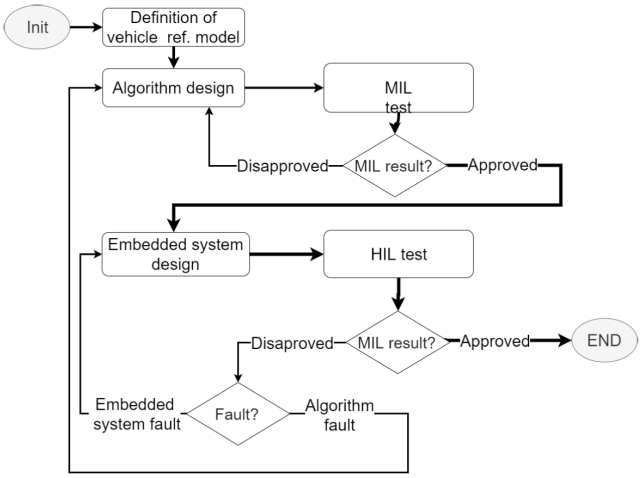

FIGURE 4. Flow chart of control development process adopted.

V. METHODOLOGY

The PIL platform was based on the framework proposed by [39]. Fig. 4 illustrates the development and evaluation process followed in this work.

As the MPC design is based on the vehicle model, the first project stage is the definition of the reference vehicle model. This model is linearized and discretized for obtaining the discrete linear model needed for MPC design. Once the reference model and the discrete linear model are defined, the control algorithm is designed and implemented as a model for computational simulation using Matlab/Simulink.

Model-in-the-loop (MIL) simulations are performed to validate the control algorithm. In MIL, the whole control system is implemented for computational simulation. And test scenarios are simulated for observation of control effectiveness. MIL simulation is performed until results show that the proposed ESC can improve lateral stability. When the results show that the lateral performance of a vehicle with ESC assistance does not meet the requirements, the algorithm is updated before the next MIL testing run.

Once the algorithm is approval in MIL tests, the proposed controller is implemented as an embedded Linux software for BeagleBoneBlack and submitted to Processor-in-the-loop simulations. In this platform, the BeagleBoneBlack executes and tests the controller together with a platform that runs a Simulink Real-Time simulation of vehicle dynamics. The whole procedure is repeated until the controller achieves the required performance on improving lateral stability. When the controller fails in embedded test due to algorithm error, the later is updated, and all the development stages since MIL

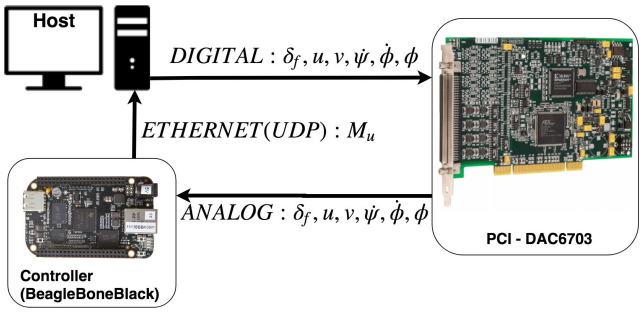

FIGURE 5. Vehicle models.

simulations are repeated. When the controller fails due to implementation error, it is fixed, and just PIL simulations are performed again.

The platform used to test the embedded control consists of a host computer, a digital-analog converter PCI-DAC6703DA2 and Ethernet connection. The host PC runs the Simulink Real-Time environment, which is a real-time simulation of vehicle response to control yaw-moment command. Simulink Real-Time provides real-time updated signals read by the controller, which are longitudinal speed, lateral speed, yaw rate, roll rate, roll angle, and front wheels steering angle. The PCI-DAC6703 is used to send such signals to the analog inputs of the controller, which is the Beaglebone Black. And Ethernet connection is used to send over User Datagram Protocol (UDP) the yaw-moment given as control input to host. Fig. 5 illustrates the proposed testbench.

A. INTELLIGENT DRIVER MODEL

The intelligent driver model presented in [40] is included in the simulation environments to compute the steering wheel angle commanded by the driver based on the vehicle states. It is important to make clear that this model is not integrated into the control algorithm and is only used to build the simulation environments.

This model considers that the driver controls the movement direction to achieve the needed trajectory for moving towards a target point A at a distance L_a. The input signals measured by the simulated driver are the current position y_{os}, the desired position y_d, and yaw angle ψ. The Fig. 7 shows the block diagram of control law used to simulate driver behavior to obtain a steering wheel angle δ_D. The parameters of this model are the distance L_a from the vehicle position to target point, actuation delay T_k, and steering gain W that represents driver expertise. Figures 6 and 7 illustrate this model.

VI. RESULTS

Simulations were performed for the double lane change (DLC) test of standard No. ISO 3888:1975 as presented in [40]. In this test, an attempt to maneuver is considered to be successful when the vehicle does not exceed the boundaries of lateral displacement from the desired path. The nonlinear model of vehicle dynamics presented in Section II is used to simulate vehicle motions. The model presented

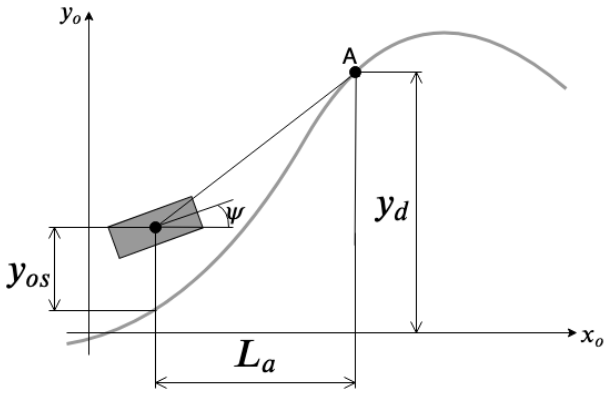

FIGURE 6. Illustration of driver modeling.

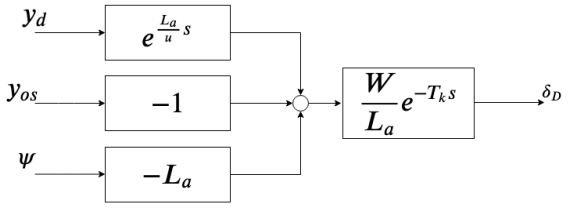

FIGURE 7. Block diagram of driver model.

TABLE 2. Parameters of simulation models of vehicle and driver.

Param.	Value	Param.	Value
a	1.1 m	b	1.3 m
t_f	1.4 m	t_r	1.41 m
h_s	0.55 m	h	0.6 m
m	1070 Kg	m_s	900 Kg
I_{zz}	2100 Kgm^2	I_{xx}	500 Kgm^2
I_{xz}	47.0 Kgm^2	I_s	20
$c_{\phi f}$	1050 Nms/rad	$c_{\phi r}$	1050 Nms/rad
$k_{\phi f}$	32795 Nm/rad	$\partial\delta_f/\partial\phi$	0.1
$k_{\phi r}$	32795 Nm/rad	$\partial\delta_r/\partial\phi$	-0.1
L_a	$1.2 \cdot u$	W	0.2
μ	0.75	T_k	0.2
a_0	1.3	a_1	-49
a_2	1216	a_3	1632
a_4	11	a_5	0.006
a_6	-0.04	a_7	-0.4
a_8	0.003	a_9	-0.002
a_{10}	0	b_0	1.57
b_1	-48	b_2	1338
b_3	5.8	b_4	444
b_5	0	b_6	0.003
b_7	-0.008	b_8	0.66
b_9	0	b_{10}	0

in Section V-A is used for generating the steering wheel commanded by an average human driver. Table 2 shows the parameters used in the simulation of vehicle dynamics. Table 3 shows the parameters of the linear model used in the implementation of the control algorithms.

The command constraint of MPC algorithm is defined to ensure that the ESC provides feasible vales of external yaw moment. The feasibility limit is defined as presented Section III, based on the limit of the longitudinal force

TABLE 3. Parameters of the linear model used in control design.

Param.	Value	Param.	Value
a	1.1 m	b	1.3 m
h_s	0.55 m	m_s	900 Kg
I_{zz}	2100 Kgm^2	I_{xx}	500 Kgm^2
I_{xz}	47.0 Kgm^2	$c_{\phi f}$	1050 Nms/rad
$c_{\phi r}$	1050 Nms/rad	u	100km/h
$k_{\phi f}$	32795 Nm/rad	$\partial\delta_f/\partial\phi$	0.1
$k_{\phi r}$	32795 Nm/rad	$\partial\delta_r^{'}/\partial\phi$	-0.1
a	1.1 m	b	1.3
$C_{\alpha fl}$	45292μ N/rad	$C_{\gamma fl}$	-86340 μ N/rad
$C_{\alpha fr}$	45292μ N/rad	$C_{\gamma fr}$	-86340μ N/rad
$C_{\alpha rl}$	39018μ N/rad	$C_{\gamma rl}$	-61455μ N/rad
$C_{\alpha rr}$	39018μ N/rad	$C_{\gamma rr}$	-61455μ N/rad
μ	0.75		

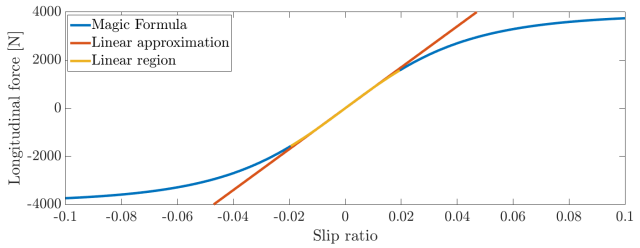

FIGURE 8. Tire's longitudinal force calculated by the Pacejka's Magic Formula and its linear approximation.

generated on tires. Figure 8 shows the chart of the Pacejka's Magic Formula, and its linear approximation for the coefficients presented in Table 2. According to this tire model, the maximum longitudinal force obtained in the linear operation of the tire is 1548N. And thus, the yaw moment obtained when the difference between the longitudinal forces of the tires on the left and right side of the vehicle is equal than 15% of 1548 N given by:

$$0.15 \cdot 1548N \cdot (t_f + t_r)/2 = 326[Nm] \tag{37}$$

in which t_f and t_r is the widths of the longitudinal and rear track, respectively.

Following the criteria presented in Section III, the constraint of the yaw moment M_{th} configured in MPC algorithm must be less than 326 [Nm]. In this sense, the configuration of M_{th} for all the tests presented in this paper is 250 [Nm].

A. CONTROLLER TUNING

In addition to testing the proposed controller, simulations are useful for tuning of controller parameters. The MPC effectiveness depends on the value of its parameters, such as the weight matrices of QP cost function, $\mathbf{Q}_u$, and $\mathbf{Q}_y$, the coefficients of exponential parameterization λ and α and the prediction horizon N. Theoretically, a long prediction horizon increases the capacity of ESC to act before a dangerous driving condition happens, and also contributes to the stability of MPC [15]. But in practical terms, the increasing of prediction horizon increases the memory required to store the QP matrices and the latency of the algorithm to solve the QP problem, which decreases the stability performance.

The proposed controller was implemented as software for embedded Linux running on ARM CORTEX A8 of BeagleBoneBlack. Th parameters $\mathbf{Q}_u$, $\mathbf{Q}_y$, λ, α and N were defined with an iterative procedure. The following procedure describes the tuning method starting with the prediction horizon $N = 15$.

1) **Tuning of $\mathbf{Q}_u$, $\mathbf{Q}_y$, ν, α:**
The control model of MIL simulation is configured with the chosen horizon. The others parameters are defined by the minimization of the accumulation of states square error, path square error and yaw moment energy, obtained from results of MIL simulation for double lane change maneuver (standard No. ISO 3888:1975 as presented in [40]) at 80km/h, 100km/h, and 120km/h.
2) **Profiling the effective computation times**
The controller is configured with the optimum parameters found in the previous step. Than it is tested embedded on the BeagleBoneBlack for each horizon $N \in [15, 20, 25, 30, 35, 40, 45, 50, 55, 60, 65]$. The profiling tool of GNU ARM embedded toolchain is used during these simulations to measure the command update time achieved for each horizon. Since, the PIL platform enables the test of update times multiple of the sampling time of the real-time simulation of vehicle response (0.8ms), the effective computation time is defined as the minimum multiple of 0.8ms greater than the measured computation time.
3) **Measure of the stability performances**
The mean square error (MSE) of the lateral displacement is measured, from results of MIL simulations of the DLC maneuver at 120km/h, for the control model configured with each prediction horizon and its effective update time measured in the previous step. The horizon that gets the smallest MSE measured is the chosen one.
4) **Completion and iteration**
The procedure repeats while the chosen horizons of the current and the last iterations are not the same.

Figure 9 shows the results obtained in the last iteration of this tuning procedure. One can see that for horizons smaller than 50 sampling times, the MSE of lateral displacement decreases as long as the horizon increases. The effect of increasing N clearly improves the system performance since model-plant mismatches are not significant, and higher prediction horizons are desirable for stability and optimally [15]. On the other hand, for $N > 50$, model uncertainties become more significant, and the closed-loop performance starts degrading since the mean square error of lateral displacement rises almost exponentially. Based on these results, the optimal prediction horizon of the proposed control scheme was set to $N = 50$.

The tables 4 and 5, show the optimal configuration obtained from the tuning procedure for the MPC algorithm implemented with a linear model that includes the roll motion

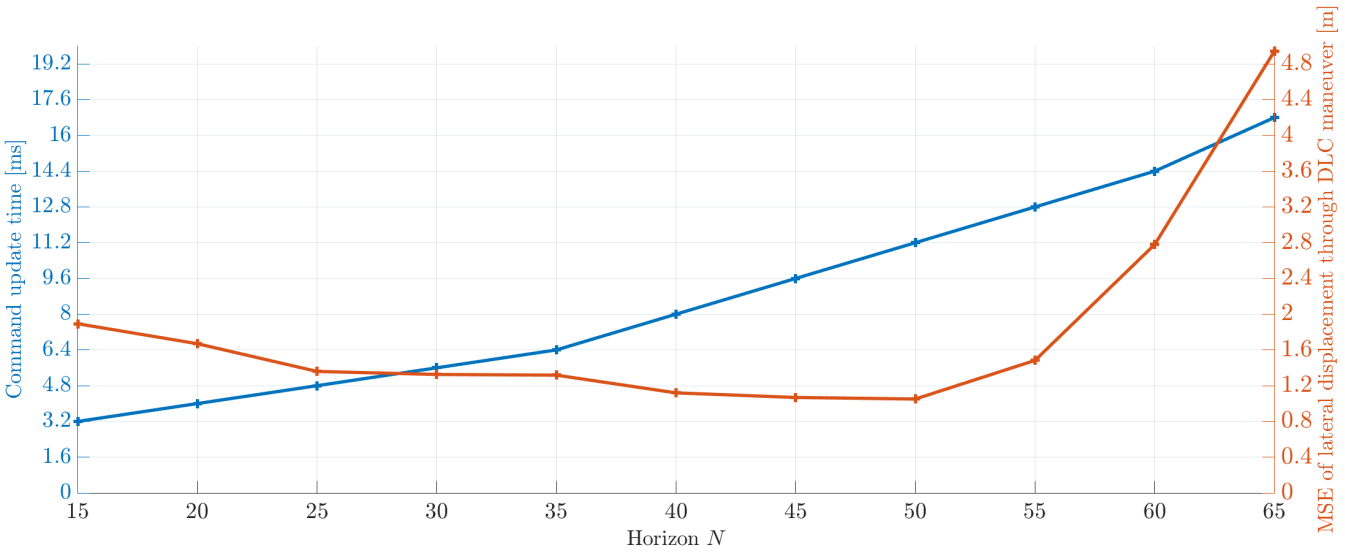

FIGURE 9. Evolution of minimum computation time and mean square error of lateral displacement depending on the prediction horizon *N*.

TABLE 4. Configuration of the MPC-based ESC implemented with a prediction model that includes the roll motion.

Param.	Value	Param.	Value
N	50 τ	τ	9.6 ms
$\mathbf{Q}_y$	$diag(1103, 1117)$	$\mathbf{Q}_u$	1e-5
λ	70510	α	6499

TABLE 5. Configuration of the MPC-based ESC implemented with a prediction model that does not include the roll motion.

Param.	Value	Param.	Value
N	50 τ	τ	9.6 ms
$\mathbf{Q}_y$	20000	$\mathbf{Q}_u$	1e-5
λ	100000	α	849

(i.e., roll control on) and with a linear model that does not include the roll motion (i.e., roll control off). In the configuration of the algorithm with roll control on, the optimal matrix Q_Y weights only errors in yaw rate and roll angle, so the regulated output matrix C_C is defined such that only these states are included within the regulated states. And in the configuration of the MPC with roll control off, the optimal $\mathbf{Q}_y$ weights only the yaw rate, thus the C_c matrix is defined such that only the yaw rate is regulated. Since the use of a simpler prediction model reduces the computational complexity of the MPC algorithm, the calculation time of 12.2 ms measured for the MPC with roll control off is smaller than the 13.6 ms measured for the MPC with roll control on.

The parameters of activation/deactivation criteria were defined from manual adjustment. Table 6 shows the configuration of the activation criteria.

This tuning procedure was also performed to find the optimal configuration for the MPC without parameterization.

TABLE 6. Configuration of the ESC activation and deactivation criteria.

Param.	Value	Param.	Value
β_{th}	0.1 rad	T_{on}	0.08 s
ψ_{eth}	0.1 rad/s	T_{off}	0.8s

However, it is worth mentioning that there is no configuration in which the MPC without parameterization, running on embedded hardware based on the ARM Cortex A8 of BeagleBoneBlack Rev C, is feasible or effective to avoid handling destabilization in real-time simulation. For this reason, only simulations using parameterized MPC are presented in this section.

In this case, to study the benefits of MPC capabilities to predict the vehicle motion and deal with command constraints, simulations also were performed for the proposed control architecture, replacing the MPC with an LQR control, as presented in [41]. The LQR was chosen because it is also an optimal control technique, that although it does not have the benefits of MPC, its control algorithm has low computational complexity that leads to higher command updating rate. This comparison is interesting because the command update time is one of the main challenges for applying the MPC in real-time applications, for which the proposed system intends to present a solution.

For a fair comparison, the LQR is set up to run with the higher update rate enabled by the PIL platform, which is the sample time of the real-time simulation of vehicle response (0.8ms). It is derived from the same linear model that MPC, and the weighting matrices $\mathbf{Q}_y$ and Q_U are optimized by the following procedure:

1) Measure the calculation time of the LQR running in the ARM Cortex A8.

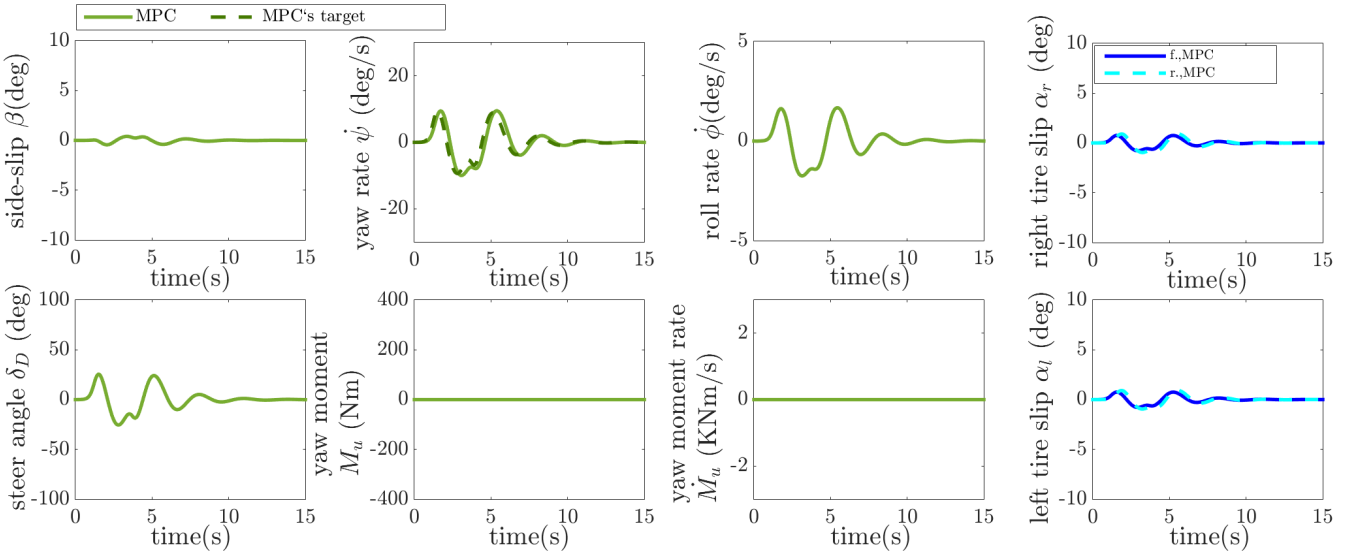

FIGURE 10. Results from MIL simulation of DLC at 80km/h for vehicle with MPC-based ESC. In this maneuver, the ESC actuation is not required. The target yaw rate is computed by Eq. 19, which depends on the driver's behavior in steering wheel control during the maneuver. The indexes f. and r. denote the front and rear tires, respectively.

TABLE 7. Configuration of the LQR-based ESC.

Param.	Value
τ	0.5 ms
$\mathbf{Q}_y$	diag(66.0, 248.9, 9.6, 374.2)
$\mathbf{Q}_u$	1e-5

2) Find the weighting matrices $\mathbf{Q}_y$ and $\mathbf{Q}_u$ that minimizes a cost function defined based on the accumulation of lateral displacement square error obtained from MIL simulations of DLC maneuvers at 80 km/h, 100 km/h and 120 km/h.

The optimization problem of the second step of the LQR tuning procedure is solved by using the Particle Swarm Optimization (PSO), to perform a global search for the optimal values, and the interior point method, to perform linear programming towards the PSO results for fine-tuning. Table 7 shows the results of LQR tuning, in which the command update period equal to 0.5 ms is 27.2 times faster than the rate obtained with the MPC with roll control on.

B. RESULTS FROM MIL SIMULATIONS

The DLC at 80 km/h was simulated, in MIL environment, for a vehicle with proposed ESC, to observe if the controller acts unnecessarily or impairs steering when a driver is able to drive without assistance. MIL simulations of DLC at higher speeds also were performed to compare the effectiveness in improving the lateral stability of LQR-based ESC, MPC-based ESC with roll control on and off, and MPC-based ESC with roll control on without the exponential parameterization applied to reduce the calculation time.

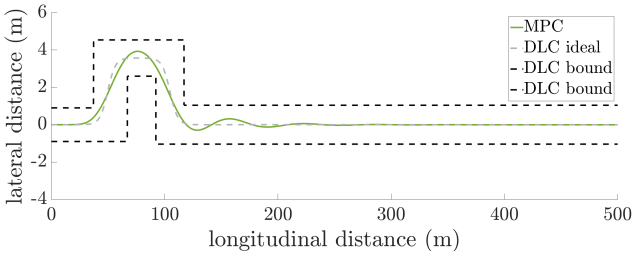

FIGURE 11. Vehicle trajectory from MIL simulation of DLC maneuver at 80 km/h.

The DLC at 80 km/h was simulated to observe if the ESC effect unnecessary interferes on steering in a scenario where the driver can perform the maneuver without ESC assistance, The Figures 10 and 11 show the result from this simulation.

1) DLC AT 80 km/h

From results shown in Fig. 10, where the yaw moment given as control signal remains equal to zero, and from the vehicle's trajectory shown on Fig. 11, where the DLC test is successfully performed, one can confirm that driver is able to perform this maneuver without ESC assistance. Therefore, the obtained yaw rate is command only by the driver steering command, and it remains close to its desired valued given by the Equation ((19)). This result indicates a coherence between models of driver, vehicle and desired yaw rate. The actuation remains null because of the control algorithms

The side-slip angle β and roll angle ϕ of the vehicle body and the tire slip angles α remain smaller than 5 degrees during all the simulation, which means that the vehicle states remains within the trust region of the vehicle-linear-prediction model.

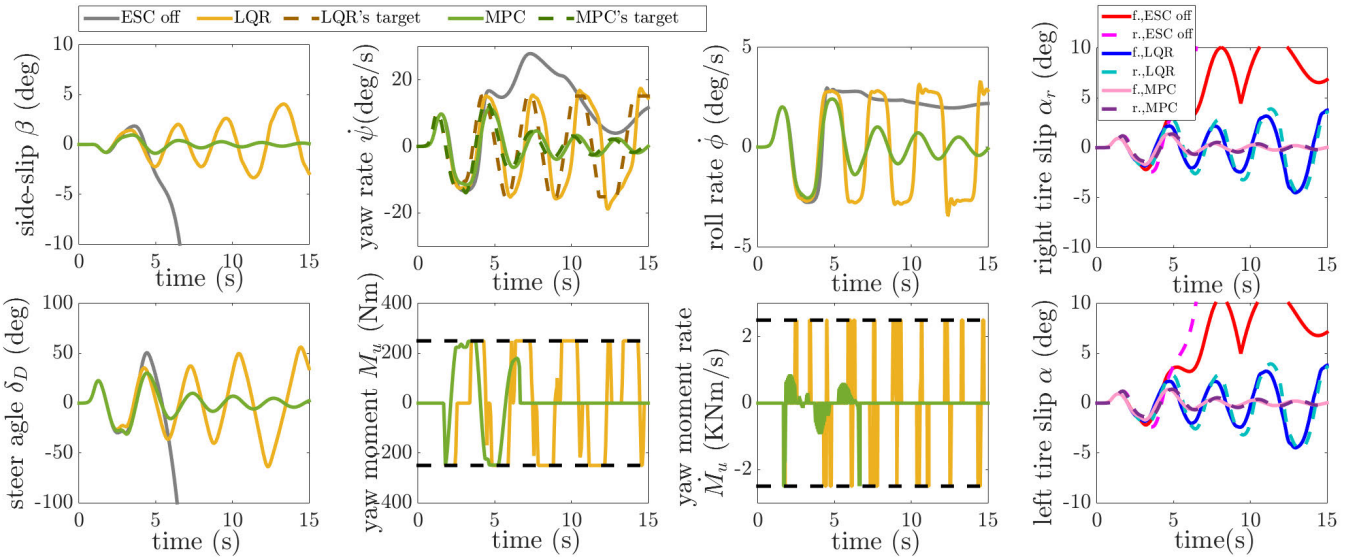

FIGURE 12. Results from MIL simulation of DLC at 100km/h for vehicle without ESC, with MPC-based ESC and with LQR-based ESC. The target yaw rates are computed by Eq. 19, which depends on the driver's behavior in steering wheel control during the maneuver. The indexes f. and r. denote the front and rear tires, respectively.

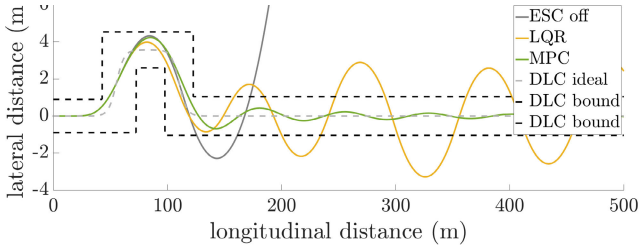

FIGURE 13. Vehicle trajectory from MIL simulation of DLC maneuver at 100 km/h for vehicles without ESC, with MPC-based ESC and with LQR-based ESC.

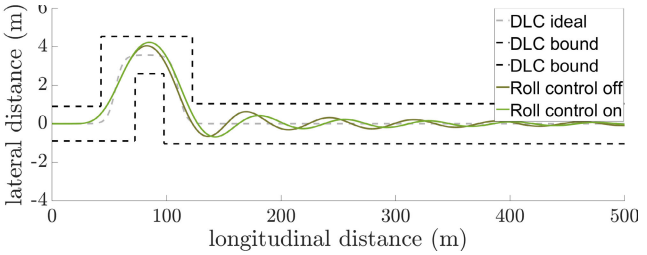

FIGURE 14. Vehicle trajectory from MIL simulation of DLC maneuver at 100 km/h for vehicles with MPC-based ESCs with roll control on and off.

2) DLC AT 100 km/h

The DLC at 100km/h was simulated to observe the ESC effectiveness in a scenario where initially the vehicle response is at the trim point of the prediction model, and the driver is not able to perform the double lane changing without assistance. The Figures 12 and 13 show the results obtained from this simulation. From the trajectory shown in Fig. 13, and side-slip, yaw rate, and roll rate angle shown in Fig. 12, one can confirm that the driver loses control of the vehicle without ESC assistance, whereas with LQR or MPC-based ESCs, the driver does not lose the vehicle control. With both controllers, the side-slip and the roll angles of the vehicle body and tires slip angle remains smaller than 5 degrees, which means that vehicle states remain in the trust region of the vehicle-linear-prediction model.

By comparing the results obtained with LQR and MPC-based ESCs shown in Fig. 12, one can see that even running at 22.4 times lower command update rate, better lateral stability improvements are achieved with the MPC since the vehicle with MPC-based ESC exhibits smaller side-slip and tire slip angles than those obtained with LQR. One can also see that the steering input in results for MPC is lower than the obtained for LQR. This means that the driver needs less effort to drive when assisted by the MPC-based ESC, i.e., better maneuverability improvement is also achieved with the MPC-based ESC.

Besides, only the vehicle equipped with the MPC-based ESC performs the maneuver without exceeding the lateral displacement limits from the desired trajectory. The LQR-based ESC exhibits a more aggressive actuation, achieving the saturation of yaw moment most of the simulation time, and, even so, it is not able to allow the maneuver without slipping away from the DLC test boundaries.

The DLC at 100 km/h also was simulated for the MPC-based ESC with roll control disabled. The Fig. 14 shows the trajectory obtained from the simulation of DLC at 100km/h performed for vehicles with proposed MPC-based ESC with roll control on and off. One can see that the vehicles equipped with both controllers are able to perform this maneuver successfully. As, in this scenario, the stability improvements achieved with both the controllers are almost the same, no benefits can be noted for the inclusion of roll control, but at least no performance losses are observed.

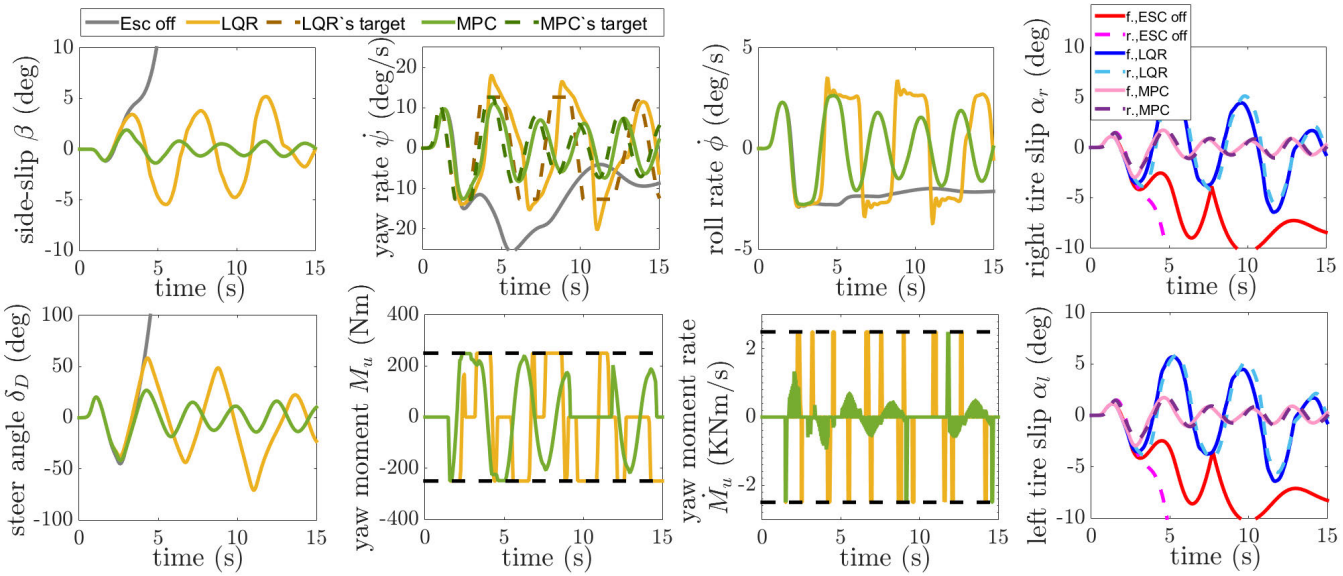

FIGURE 15. Results from MIL simulation of DLC at 120km/h for vehicles without ESC, with MPC-based ESC and with LQR-based ESC. The target yaw rates are computed by Eq. 19, which depends on the driver's behavior in steering wheel control during the maneuver. The indexes f. and r. denote the front and rear tires, respectively.

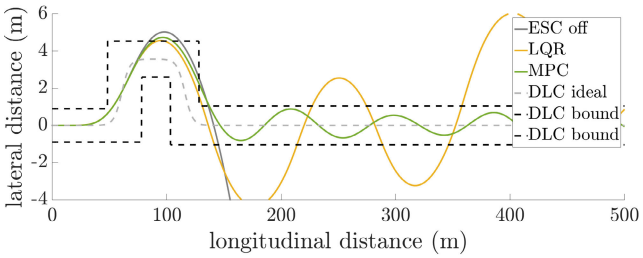

FIGURE 16. Vehicle trajectory from MIL simulation of DLC maneuver at 120 km/h for vehicles without ESC, with MPC-based ESC and with LQR-based ESC.

3) DLC AT 120 km/h

The DLC at 120km/h was simulated to test the ESC on control of the vehicle at a higher speed than the trim point of the prediction model. The Figures 15 and 16 show the results obtained for vehicles without ESC assistance, and with LQR and MPC-based ESC.

From the trajectory shown in Fig. 16, obtained for the vehicle without ESC, one can see that the driver is not able to perform the double lane changing at 120 km/h without losing the vehicle control. The trajectories obtained with LQR and MPC-based ESCs have different performances, but with both controllers, the results show that the driver does not lose vehicle control. The vehicle with LQR-based ESC exhibits a rude escape from DLC boundaries, whereas the vehicle with MPC-based ESC briefly crosses the bounds of DLC once at the exiting of the second lane changing.

From the results shown 15, it is possible to see that the MPC-based ESC exhibits a softer actuation on yaw moment input, and is still more efficient in reducing of side-slip and roll angles error. With the MPC-base ESC, the side slip and roll angles of the vehicle body and the tire slip angles remain smaller than 5 degrees, which means that the effectiveness of the stability control keeps the vehicle states in the trust region of the vehicle-prediction-linear model.

The DLC at 120 km/h also was simulated for the MPC-based ESC with roll control disabled. The results obtained with roll control on and off are presented Fig. 17 and Fig. 18. From which one can see the benefits of including roll control, since the trajectory presented in in Fig. 18 obtained from simulation with roll control off exhibits a larger error at the exit of the second lane changing than the obtained with roll control on. In the states of vehile dynamics presented in Fig. 17 obtained from these simulations, one can see that the vehicle equiped with an ESC without roll control has a higher roll rate, which means a higher risk of rollover and lower passenger comfort. In addition to the extra roll rate, the vehicle without roll control also has a higher yaw rate, side-slipping, and tire-slipping, which means a lower stability performance. And comparing the energy of the steer angle signal controlled by the driver, the amplitude without roll control is greater than with roll control, which means that the driver needs to make an extra effort to maneuver. Therefore, in this scenario, stability performance is greatly improved by the inclusion of roll control.

The increased influence of roll motion on the vehicle at high speeds is theatrically expected, because, at higher speeds, the roll rate has a stronger influence on yaw rate and tire dynamics, because it affects the vertical load transference between tires, which changes the lateral force acting on tires.

4) DLC AT 110 km/h WITH VEHICLE PARAMETERS DIVERTING FROM PREDICTION MODEL

The effectiveness of proposed controller on a vehicle whose response is different from that predicted by linear model also is evaluated. MIL simulation was performed for DLC at 110km. Besides the different speed, the vehicle simulated in

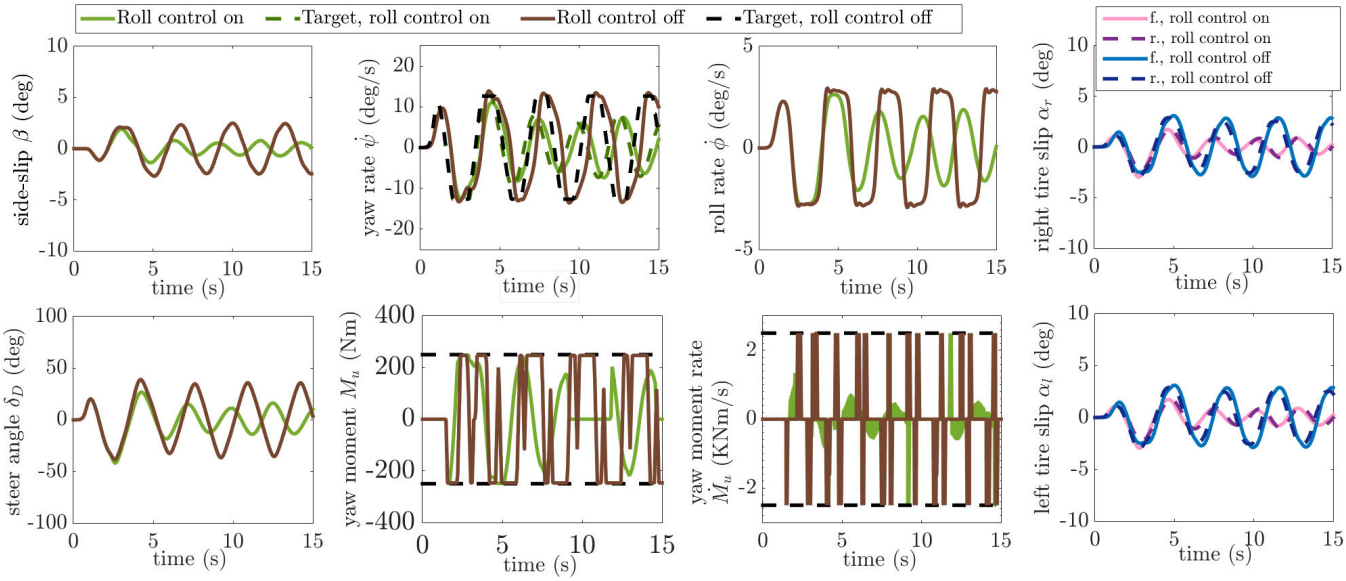

FIGURE 17. Results from MIL simulation of DLC at 120km/h for vehicles with MPC-based ESCs with roll control on and off.The target yaw rates are computed by Eq. 19, which depends on the driver's behavior in steering wheel control during the maneuver. The indexes f. and r. denote the front and rear tires, respectively.

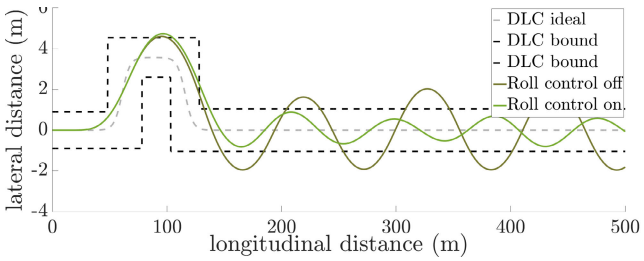

FIGURE 18. Vehicle trajectory from MIL simulation of DLC maneuver at 120 km/h for vehicles with MPC-based ESCs with and with roll control on and off.

this scenario has mass, center of mass position and tire-road friction different from values assumed by control algorithms. Parameters used in this simulation are shown in Table 8, parameters not shown in this table are equal to parameters shown on Table 2. The Fig. 19 shows results from this simulation. It is possible to see that performance decreases in comparison with vehicle whose parameters match the prediction model's parameters, but ESC remains effective in prevent the driver from losing the control.

C. RESULTS FROM EMBEDDED SIMULATIONS

The PIL simulations were performed to test the algorithm running on ARM Cortex A8 of BeagleBoneBlack Rev C, with 0.8ms sample time of feedback signals. This sampling time is the fastest rate achieved by the platform running a real-time simulation of vehicle response. The Figure 20 shows the results obtained from this simulation of DLC at 110 Km/h. Besides disturbances in acquisition of feedback signals read by the controller through analog inputs, this scenario test the control in presence of disturbances in vehicle response

TABLE 8. Parameters of simulated vehicle configured in tests of MPC-based ESC in presence of prediction model uncertainties. This table shows the non-nominal parameters and their deviations (column Dev.) from the nominal values shown in the table 2.

Param.	Value	Dev.	Param.	Value	Dev.
a	1.096 m	-5.5%	m	1177 Kg	10%
b	1.306 m	4.6%	μ	0.675	10 %

in respect with prediction model, due to difference between simulated vehicle speed and constant speed assumed by prediction model.

The Figure 20 shows the results from PIL simulation in comparison with MIL simulation. The control signal observed in MIL and PIL simulations are different from each other. This can be understood as the effect of disturbances in control activation when errors are close to decision threshold. However, from observation of yaw and roll rates, side-slip angle and the trajectory during maneuver, one can see that performance in embedded testing is close to the observed in MIL simulation.

1) COMPARISON BETWEEN MPC-BASED ESCs WITH AND WITHOUT PARAMETERIZATION

To demonstrate the benefits of exponential parameterization, DLC maneuver at 120 km/h was simulated for MPC-based ESC, with roll control, and without parameterization. In such a scenario, the computation time increased from 13.6 ms to 231 ms. The trajectory obtained from this simulation is shown in Figure 21, where only the MPC with exponential parameterization is effective in avoiding the instability. This

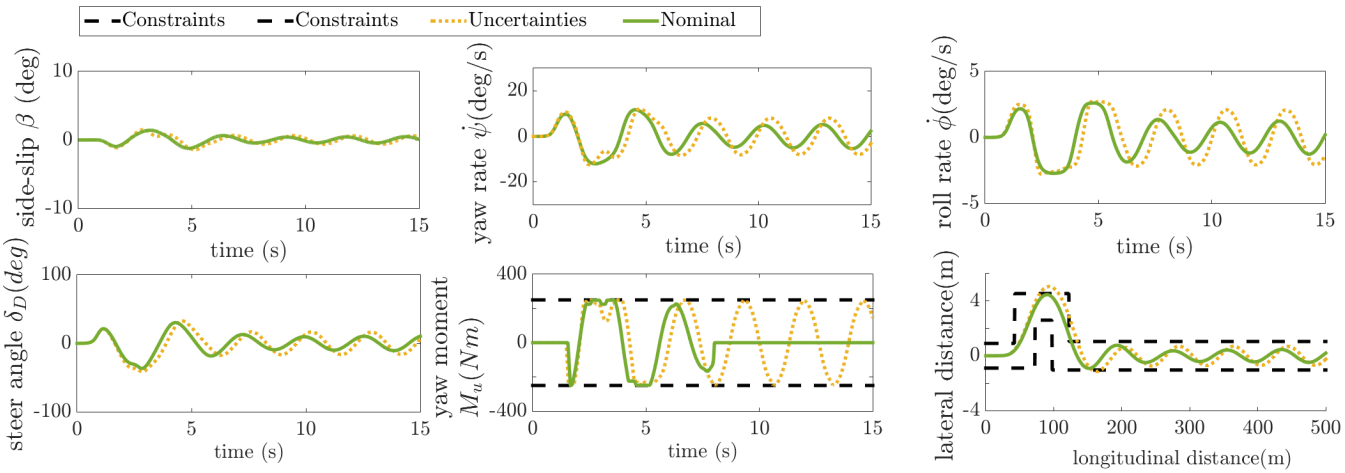

FIGURE 19. Results from MIL simulation of DLC at 110km/h with parameters equal the nominal values assumed by prediction model, and with prediction model uncertainties. In the simulation model uncertainties, the simulated vehicle is configured with non-nominal CG position, mass and tire-road friction shown on Table 8.

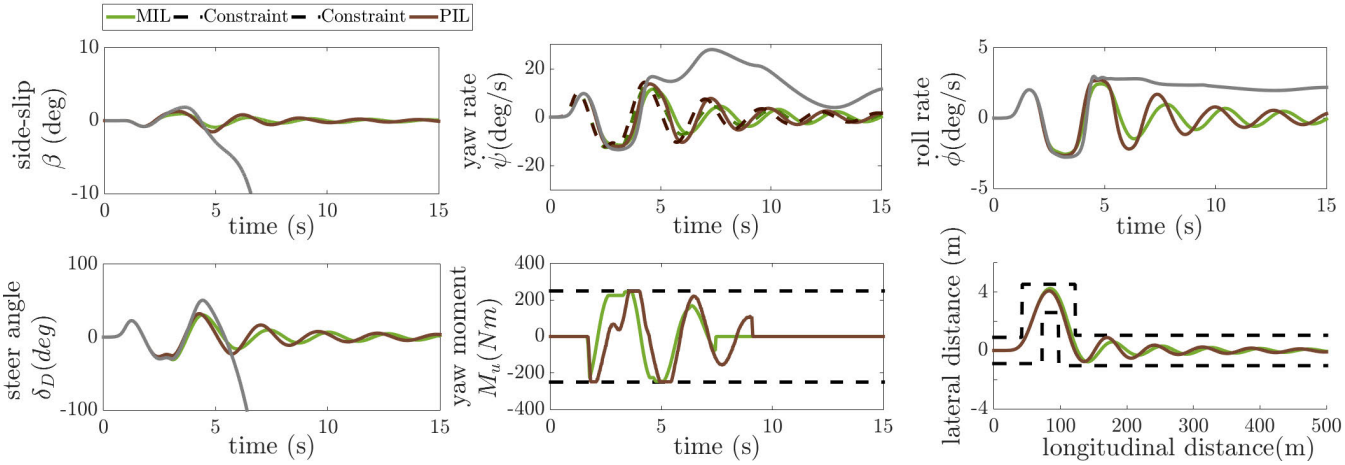

FIGURE 20. Results from PIL and MIL simulation of DLC at 110 km/h.The target yaw rates are computed by Eq. 19, which depends on the driver's behavior in steering wheel control during the maneuver.

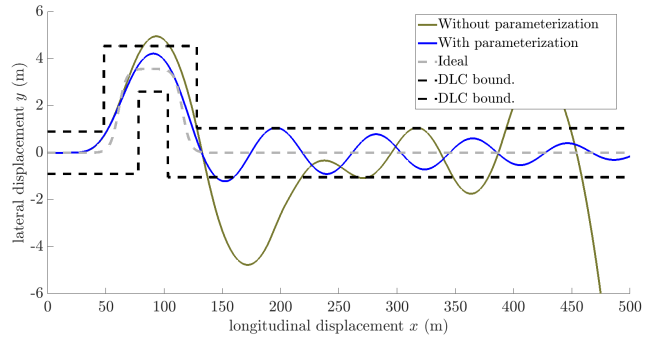

FIGURE 21. Vehicle trajectory from MIL simulation of DLC maneuver at 120 km/h for MPC-based ESC with roll control with exponential parameterization, whose calculation time is equal to 13.6 ms, and without parameterization, whose calculation time is equal to 231.2 ms.

is because the control without parameterization has an insufficient update rate of the commands.

VII. CONCLUSION

In this paper, a parameterized constrained MPC strategy for an upper-level ESC system was presented and discussed. The proposed approach uses as a prediction model, a 3DOF model that considers lateral, yaw, and roll motions linearized for constant longitudinal speed and considering small roll and side-slip angles. The main contribution of this work lies in to use exponential parameterization of the input vector to reduce the complexity of the optimization problem without loss of performance. The parameterization contributes to reducing the computation time from 231.2 ms to 13.6, and thanks to that, the stability performance is increased. Thus, this approach makes it possible to implement this control strategy in commercial vehicles that have limited processing hardware. Results from the embedded testing show that the proposed control algorithm is computationally efficient for real-time applications, even running in a hardware with limited resources. These results

also demonstrated the controller's robustness to acquisition system errors.

The results obtained from MIL simulations show that the proposed algorithm does not interfere when it is not required; it can prevent the driver from losing control of the vehicle. Moreover, its performance remains in the presence of disturbances in vehicle response with respect to a prediction model. The stability improvement achieved by addressing the MPC technique was better than the obtained with similar LQR-based ESC. The comparison between for DLC at 100 km/h and 120 km/h indicates that for lower speeds, the performance of ESC with and without roll control is almost the same. For higher values of speed, the enabling of roll control considerably improves the stability performance without significant changes regarding the computational cost of proposed MPC-based ESC.

Future works consist of implementing a real-time estimation of the tire-road friction coefficient by replacing the actual fixed value used in the tire model. Another point to investigate is to develop a lower-level algorithm to control rotation torque of each wheel, such that the resultant yaw moment equals the correcting yaw moment. Further works will also investigate the use of a lateral stability index to analyze the control performance to re-define the control objectives and the ESC activation criteria.

ACKNOWLEDGMENT

The authors acknowledge the Coordination of Superior Level Staff Improvement (CAPES), the National Council for Scientific and Technological Development (CNPq), and the Federal District Research Support Foundation (FAP-DF) for the financial support of this work.

REFERENCES

[1] A. Høye, "The effects of electronic stability control (ESC) on crashes—An update," *Accident Anal. Prevention*, vol. 43, no. 3, pp. 1148–1159, May 2011.

[2] L. Zhai, T. Sun, and J. Wang, "Electronic stability control based on motor driving and braking torque distribution for a four in-wheel motor drive electric vehicle," *IEEE Trans. Veh. Technol.*, vol. 65, no. 6, pp. 4726–4739, Jun. 2016.

[3] K. Chen, B. Yang, X. Pei, and X. Guo, "Hierarchical control strategy towards safe driving of autonomous vehicles," *J. Intell. Fuzzy Syst.*, vol. 34, no. 4, pp. 2197–2212, Apr. 2018.

[4] L. Li, Y. Lu, R. Wang, and J. Chen, "A three-dimensional dynamics control framework of vehicle lateral stability and rollover prevention via active braking with MPC," *IEEE Trans. Ind. Electron.*, vol. 64, no. 4, pp. 3389–3401, Apr. 2017.

[5] S. Cheng, L. Li, S. Member, H.-Q. Guo, Z.-G. Chen, and P. Song, "Stability adaptive control system based on MPC of autonomous vehicles," *IEEE Trans. Intell. Transp. Syst.*, vol. 21, no. 6, pp. 2376–2385, Jun. 2019.

[6] H. Zhou, F. Jia, H. Jing, Z. Liu, and L. Güvenç, "Coordinated longitudinal and lateral motion control for four wheel independent motor-drive electric vehicle," *IEEE Trans. Veh. Technol.*, vol. 67, no. 5, pp. 3782–3790, May 2018.

[7] M. B. Alberding, J. Tjønnås, and T. A. Johansen, "Integration of vehicle yaw stabilisation and rollover prevention through nonlinear hierarchical control allocation," *Veh. Syst. Dyn.*, vol. 52, no. 12, pp. 1607–1621, Dec. 2014.

[8] L. Shi, H. Wang, Y. Huang, X. Jin, and S. Yang, "A novel integral terminal sliding mode control of yaw stability for steer-by-wire vehicles," in *Proc. 37th Chin. Control Conf. (CCC)*, Jul. 2018, pp. 7787–7792.

[9] M. Liu, J. Huang, and M. Chao, "Multi-states combination nonlinear control of in-wheel-motor-drive vehicle dynamics stability," *Energy Proc.*, vol. 105, pp. 2746–2752, May 2017.

[10] A.-T. Le and C.-K. Chen, "Adaptive sliding mode control for a vehicle stability system," in *Proc. Int. Conf. Connected Veh. Expo (ICCVE)*, Oct. 2015, pp. 214–219.

[11] R. Rajamani and D. N. Piyabongkarn, "New paradigms for the integration of yaw stability and rollover prevention functions in vehicle stability control," *IEEE Trans. Intell. Transp. Syst.*, vol. 14, no. 1, pp. 249–261, Mar. 2013.

[12] H. Zhou and Z. Liu, "Vehicle yaw stability-control system design based on sliding mode and backstepping control approach," *IEEE Trans. Veh. Technol.*, vol. 59, no. 7, pp. 3674–3678, Sep. 2010.

[13] X. J. Jin, G. Yin, and N. Chen, "Gain-scheduled robust control for lateral stability of four-wheel-independent-drive electric vehicles via linear parameter-varying technique," *Mechatronics*, vol. 30, pp. 286–296, Sep. 2015.

[14] X. Jin, G. Yin, X. Zeng, and J. Chen, "Robust gain-scheduled output feedback yaw stability control for in-wheel-motor-driven electric vehicles with external yaw-moment," *J. Franklin Inst.*, vol. 355, no. 18, pp. 9271–9297, Dec. 2018.

[15] D. Q. Mayne, J. B. Rawlings, C. V. Rao, and P. O. M. Scokaert, "Constrained model predictive control: Stability and optimality," *Automatica*, vol. 36, no. 6, pp. 789–814, 2000.

[16] M. Alamir, *A Pragmatic Story of Model Predictive Control: Self-Contained Algorithms and Case-Studies*. Scotts Valley, CA, USA: CreateSpace Independent Publishing Platform, 2013.

[17] A. Nahidi, A. Kasaiezadeh, S. Khosravani, A. Khajepour, S.-K. Chen, and B. Litkouhi, "Modular integrated longitudinal and lateral vehicle stability control for electric vehicles," *Mechatronics*, vol. 44, pp. 60–70, Jun. 2017.

[18] M. Ataei, A. Khajepour, and S. Jeon, "Reconfigurable integrated stability control for four- and three-wheeled urban vehicles with flexible combinations of actuation systems," *IEEE/ASME Trans. Mechatronics*, vol. 23, no. 5, pp. 2031–2041, Oct. 2018.

[19] H. Guo, F. Liu, F. Xu, H. Chen, D. Cao, and Y. Ji, "Nonlinear model predictive lateral stability control of active chassis for intelligent vehicles and its FPGA implementation," *IEEE Trans. Syst., Man, Cybern. Syst.*, vol. 49, no. 1, pp. 2–13, Jan. 2019.

[20] M. Jalali, E. Hashemi, A. Khajepour, and S.-K. Chen, "A combined-slip predictive control of vehicle stability with experimental verification," *Veh. Syst. Dyn.*, vol. 56, no. 2, pp. 319–340, 2017.

[21] Y. Zheng and B. Shyrokau, "A real-time nonlinear MPC for extreme lateral stabilization of passenger vehicles," in *Proc. IEEE Int. Conf. Mechatronics (ICM)*, Mar. 2019, pp. 519–524.

[22] M. Ataei, A. Khajepour, and S. Jeon, "Model predictive control for integrated lateral stability, traction/braking control, and rollover prevention of electric vehicles," *Veh. Syst. Dyn.*, vol. 58, no. 1, pp. 49–73, Jan. 2019.

[23] M. Jalali, A. Khajepour, S.-K. Chen, and B. Litkouhi, "Integrated stability and traction control for electric vehicles using model predictive control," *Control Eng. Pract.*, vol. 54, pp. 256–266, Sep. 2016.

[24] M. Jalali, E. Hashemi, A. Khajepour, S.-K. Chen, and B. Litkouhi, "Integrated model predictive control and velocity estimation of electric vehicles," *Mechatronics*, vol. 46, pp. 84–100, Oct. 2017.

[25] M. Jalali, S. Khosravani, A. Khajepour, S.-K. Chen, and B. Litkouhi, "Model predictive control of vehicle stability using coordinated active steering and differential brakes," *Mechatronics*, vol. 48, pp. 30–41, Dec. 2017.

[26] M. Choi and S. B. Choi, "Model predictive control for vehicle yaw stability with practical concerns," *IEEE Trans. Veh. Technol.*, vol. 63, no. 8, pp. 3539–3548, Oct. 2014.

[27] M. Ataei, A. Khajepour, and S. Jeon, "A novel reconfigurable integrated vehicle stability control with omni actuation systems," *IEEE Trans. Veh. Technol.*, vol. 67, no. 4, pp. 2945–2957, Apr. 2018.

[28] M. R. Licea and I. Cervantes, "Robust indirect-defined envelope control for rollover and lateral skid prevention," *Control Eng. Pract.*, vol. 61, pp. 149–162, Apr. 2017.

[29] H. Dahmani, O. Pagès, and A. El Hajjaji, "Observer-based state feedback control for vehicle chassis stability in critical situations," *IEEE Trans. Control Syst. Technol.*, vol. 24, no. 2, pp. 636–643, Mar. 2015.

[30] B. Mashadi, M. Majidi, and H. P. Dizaji, "Optimal vehicle dynamics controller design using a four-degrees-of-freedom model," *Proc. Inst. Mech. Eng., D, J. Automobile Eng.*, vol. 224, no. 5, pp. 645–659, May 2010.

[31] S. Zheng, H. Tang, Z. Han, and Y. Zhang, "Controller design for vehicle stability enhancement," *Control Eng. Pract.*, vol. 14, no. 12, pp. 1413–1421, 2006.
[32] S. Li, D. Zhao, L. Zhang, and Y. Tian, "Lateral stability control system based on cooperative torque distribution for a four in-wheel motor drive electric vehicle," in *Proc. 36th Chin. Control Conf. (CCC)*, vol. 105, Dalian, China, Jul. 2017, pp. 2825–2830.
[33] C. Jin, L. Shao, C. Lex, and A. Eichberger, "Vehicle side slip angle observation with road friction adaptation," *IFAC-PapersOnLine*, vol. 50, no. 1, pp. 3406–3411, Jul. 2017.
[34] Y. Guo, H. Guo, Z. Yin, M. Cui, and H. Chen, "Vehicle lateral stability controller design for critical running conditions using NMPC based on vehicle dynamics safety envelope," in *Proc. IEEE Int. Symp. Circuits Syst. (ISCAS)*, May 2019, pp. 1–8.
[35] H. B. Pacejka, *Tyre and Vehicle Dynamics*, 2nd ed. Oxford, U.K.: Butterworth-Heinemann, 2006.
[36] T. Gillespie, *Fundamentals of Vehicle Dynamics* (Premiere Series Bks). Warrendale, PA, USA: SAE, 1992. [Online]. Available: https://books.google.com.br/books?id=L6xd0nx5KbwC
[37] I. Yogurtcu, S. Solmaz, and S. C. Baslamish, "Lateral stability control based on active motor torque control for electric and hybrid vehicles," in *Proc. IEEE Eur. Modelling Symp. (EMS)*, Oct. 2015, pp. 213–218.
[38] M. Alamir, *Stabilization of Nonlinear Systems Using Receding-Horizon Control Schemes: A Parametrized Approach for Fast Systems*, vol. 339. Jan. 2006. [Online]. Available: https://www.researchgate.net/publication/321610406_Stabilization_of_Nonlinear_Systems_Using_Receding-horizon_Control_Schemes_A_Parametrized_Approach_for_Fast_Systems/citation/download, doi: 10.1007/978-1-84628-471-7.
[39] A. B. C. De Farias, R. S. Rodrigues, A. Murilo, R. V. Lopes, and S. Avila, "Low-cost hardware-in-the-loop platform for embedded control strategies simulation," *IEEE Access*, vol. 7, pp. 111499–111512, 2019.
[40] A. Reński, "Identification of driver model parameters," *Int. J. Occupational Saf. Ergonom.*, vol. 7, no. 1, pp. 79–92, Jan. 2001.
[41] Z. Magalhães, A. Murilo, and R. V. Lopes, "Development and evaluation with MIL and HIL simulations of a LQR-based upper-level electronic stability control," *J. Brazilian Soc. Mech. Sci. Eng.*, vol. 41, no. 8, p. 327, Jul. 2019, doi: 10.1007/s40430-019-1808-6.

ZOÉ ROBERTO MAGALHÃES JÚNIOR received the B.Sc. degree in electronics engineering and the master's degree from the University of Brasília, Brasília, Brazil, in 2014 and 2020, respectively. Since 2014, he has been working with development of embedded firmware for automotive tracking, based on cellular and satellite communication. His main research interests include control theory and applications, automotive electronics, embedded systems, digital communication, and digital signal processing.

ANDRÉ MURILO received the degree in mechatronic engineering from the Pontifical Catholic University of Minas Gerais, in 2001, and the master's and Ph.D. degrees in automatic control from the Institut National Polytechique de Grenoble (INPG), France, in 2006 and 2009, respectively. He is currently an Associate Professor with the Faculty of Gama (UnB Gama), Universidade de Brasília. He has experience in the areas of predictive control, automotive control systems, process control, nonlinear systems, robotics, mechatronics, and industrial automation.

RENATO VILELA LOPES received the B.Sc. degree in electrical engineering from São Paulo State University (UNESP), Ilha Solteira, Brazil, in 2004, the master's degree in automated systems and control from the Instituto Tecnológico de Aeronáutica, São José dos Campos, Brazil, in 2006, and the Ph.D. degree in hybrid systems identification from the University of Brasília, Brazil, in 2014. In 2011, he joined the UnB Gama College, UnB, where he is currently an Associate Professor. His research interests include control theory and applications, systems identification, hybrid systems, estimation, and nonlinear filtering.